GAS SENSING, OPTICAL & DIELECTRIC PROPERTIES OF SPINEL STRUCTURED $Mg_{1-x}Zn_xFe_2O_4$ NANOPARTICLES

IQRA NAZIR

MPhil Physics

NUST201361972MSNS78113F

Supervised by

Associate Professor (SCME)

DR. IFTIKHAR HUSSAIN GUL

School of Natural Sciences (SNS)

National University of Science and Technology, Islamabad (NUST)

2016

This dissertation is dedicated

To

My Loving Parents.

For their endless support and encouragement.

"I couldn't Have Done It without Them"

Acknowledgements

First and foremost, I would like to thank **Allah Almighty** for His countless blessings, the one who is the most deserving of thanks and praise, may He be glorified and exalted. Blessings be upon His beloved **Prophet Hazrat Muhammad (P.B.U.H)** the last Messenger, the illuminating light and the Mercy of a mankind.

I owe my deepest gratitude to my research supervisor, **Dr. Iftikhar Hussain Gul** for all his help, patience, affectionate guidance and efficient supervision at each and every stage of this research work. His enthusiasm and valuable suggestions has been the major driving force for my research work. I would also like to acknowledge my guidance and evaluation committee (GEC) members **Dr. Zakir Hussain** and **Dr. Adeel Umer** for their insight comments and valuable guidance.

I am gratifying to the Principal of "School of Natural sciences" **Prof. Dr. Azad Akhter Siddiqui** and Head of the Department of physics **Dr. Ayesha Khalique** for their support. I am also grateful to all the faculty members and non-teaching staff for the help provided to me at various stages to accomplish this work. A very special thanks to my friends Samira Yasmin, Maryam bibi and Maryam Kiani who were always with me to share every thick and thin during this time and my lab fellows at Thermal Treatment lab SCME for their cooperation during my research. I would also like to acknowledge the beautiful moments spent with Samira Yasmin.

Furthermore, I greatly acknowledge the facilities and technical support provided at School of Chemical and Material Engineering and School of Mechanical and Manufacturing Engineering for giving me permission to use their labs and work throughout my research.

Iqra Nazir

CONTENTS

CHAPTER 4 RESULTS, ANALYSIS AND DISCUSSION

List of figures

List of tables

Abstract

Spinel ferrites are very important electronic materials because of their electrical, magnetic, optical and gas sensing properties. $Mg_{1-x}Zn_xFe_2O_4$ nanoparticles where x=0.0, 0.2, 0.35, 0.5, were synthesized by means of wet chemical Co-precipitation process. For characterization of Nano ferrites, X-ray diffraction, FTIR, SEM, UV-Visible spectroscopy, dielectric and gas sensing measurements were employed. Lattice constant and average crystallite sizes were found to be ~ $8.3A^0$ and ~ 13.2 nm respectively. These structural features are found to have significant influence on the gas sensing performances of $Mg_{1-x}Zn_xFe_2O_4$ Nano ferrites. UV– Vis absorption spectroscopy showed that the energy band gap of the synthesized Mg_{1-x} $Zn_xFe_2O_4$ nanoparticles decreases by increasing doping contents from 2.49 to 2.16 eV. Dielectric study showed a very low dielectric loss of Zn doped magnesium ferrites at frequencies over 10 MHz. It follows that samples with the composition *x*=0.5 has not only a uniformly low dielectric constant at all frequencies, it also shows a low loss factor. Differences in particle and dielectric parameters of the ferrite nanoparticles synthesized by different concentration of dopants were observed. Furthermore the gas sensing characteristics of Zn doped Mg ferrites for several gases were gained by measuring the resistance as a function of different factors, like composition and response time in air and in the presence of gas. The sensitivity of spinel Mg-Zn ferrite to gases CO_2, O_2 and N_2 at room temperature has been compared. The preliminary results have shown that the effects of Zn ions in Mg ferrite on gas sensitivity can be related with the reduction in porosity. It was observed that the gas sensitivity depends on types of semiconducting material, concentration of dopants and test gases to be detected. The nanostructured $Mg_{1-x}Zn_xFe_2O_4$ exhibited high sensitivity in order of $CO_2>O_2>>N_2$ and showed good response time of (~1min) to CO_2, demonstrated that this expanse of research can be used in the field of gas sensors devising high sensitivity and good selectivity at room temperature.

GRAPHICAL ABSTRACT

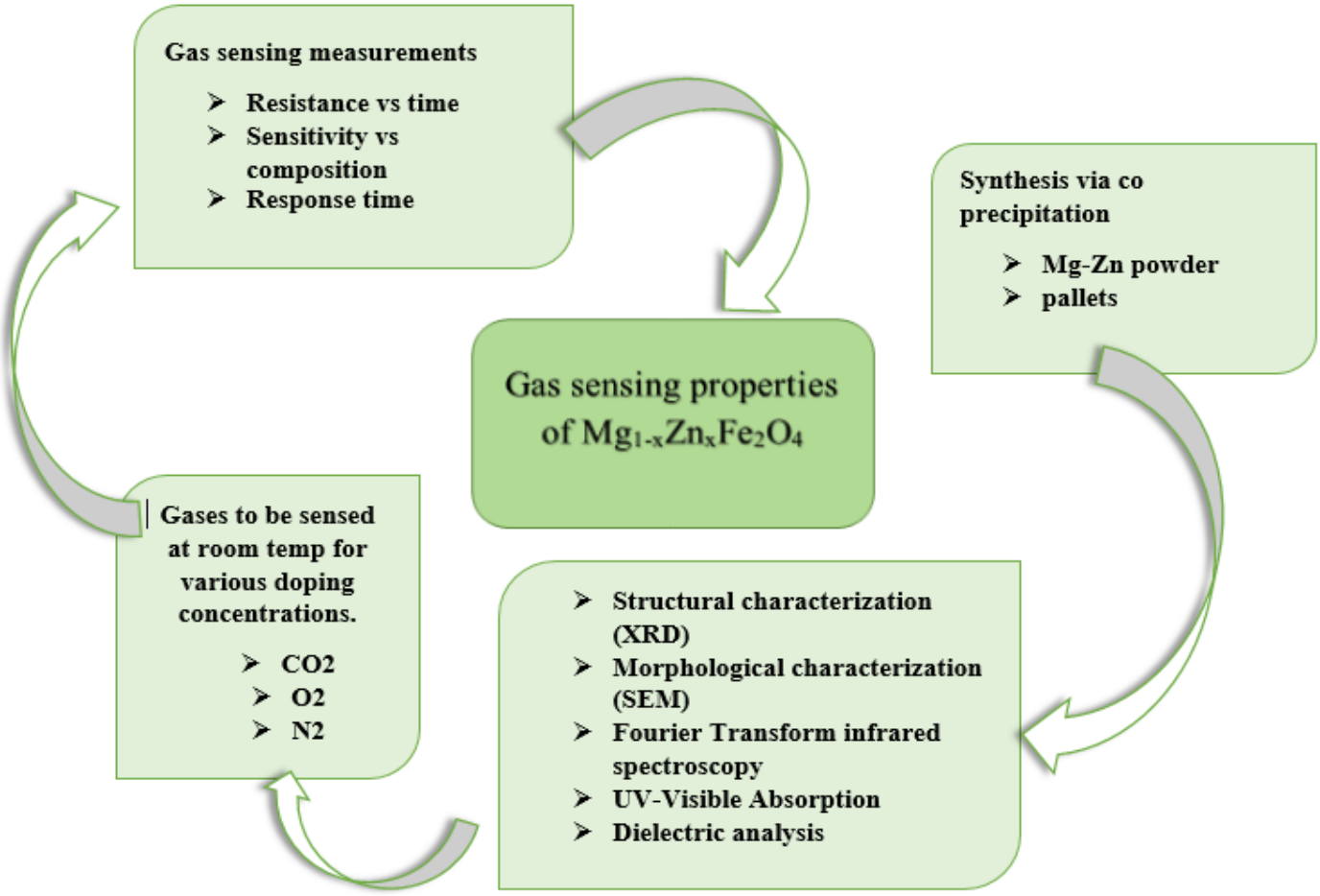

Motivation and Objectives

- To synthesize $Mg_{1-x}Zn_xFe_2O_4$ Nano ferrites as nanostructured spinel ferrites are the developing materials for various applications, through co-precipitation process which is a simple and low cost synthesis technique and to examine its structural, optical, dielectric as well as surface morphological properties of Mg-Zn ferrite.
- To study its gas sensing properties at room temperature and to gain knowledge about their interaction with the target gases.
- Therefore, the key objective of our work is to synthesize nanomaterials that may exhibits good sensitivity at room temperature and more linear sensing characteristics.

LAYOUT OF THE THESIS

The thesis is divided into five chapters. The layout of this thesis is as follows:

Chapter 1

Includes history of nanomaterials, Introduction to nanotechnology, along with its general properties and various applications.

Chapter 2

Second chapter contains literature survey comprises of introduction to spinel ferrites and its crystal structure and synthesis techniques. Further this chapter gives introduction to recent development of sensors, its limitations, Sensing principle and extensive survey on the development of sensing material.

Chapter 3

Comprises of Experimental setup to be adopted, theory of the operation and characterization techniques for the fabrication of ferrite nanoparticles.

Chapter 4

Structural, dielectric, optical, morphological, and gas sensing properties of $Mg_{1-x}Zn_xFe_2O_4$ nanoparticles were discussed in detail in this chapter.

Chapter 5

Deals with the summary of the work done and the concluding remarks drawn from the present research work. Future scope for further research work in the field of Nano sized materials as gas sensor has been given in the chapter.

CHAPTER 1

INTRODUCTION

1.1 History of Nanoscience

The history of nanotechnology, in some sense dates back to early times when humans made use of naturally-occurring nanoscale components.

1959 An American physicist Richard Feynman gave a talk, "There's Plenty of Room at the Bottom," at an American Physical Society meeting at Caltech on December 29, 1959, which is regularly held to have provided motivation for the field of nanotechnology. He had described a method by which the ability to employ individual atoms could be established. These developments show that the retroactive discovery of Feynman's gave an enveloped history that provided a link to the virtuous of Richard Feynman. Feynman's importance as a Nobel laureate and as an iconic symbol in science surely aided followers of nanotechnology and provided a valuable link to the earlier time [1]. **1974** Norio Taniguchi, The Japanese scientist was the first to use the term "Nano-technology" to describe semiconductor methods such as thin film deposition displaying control on the scale of a nanometer. According to him, "'Nano-technology' mainly consists of the handling of, separation, deformation and consolidation of materials by one atom or molecule [2].

1980's The idea of nanotechnology as a deterministic, rather than stochastic, handling of individual atoms and molecules was conceptually explored in depth by K. Eric Drexler , who promoted the technological significance of nano-scale phenomena and devices through speeches and two influential books.1990 First nanotechnology journal Japan's STA begins funding nanotech projects [3]

1990-1999 First Feynman Prize in Nanotechnology awarded for displaying a hydrogen abstraction tool in nanotechnology. Feynman Grand Prize of $250,000 was declared for synthesis of complex 3D structures with DNA molecules. First DNA-based Nano mechanical device was exhibited in

first NSF forum held with Foresight Conference. In first Nano bio conference, NASA starts work in computational nanotech.

2000-2010 First state research initiative: In California, $100 million Feynman Prize was awarded for computational materials science and for constructing a molecular switch, for using DNA to permit the self-assembly of new Nano structures and for evolving our aptitude to prototype molecular appliance systems. Roco declares Nano machine project sum has touched 300 Feynman Prize in Nanotechnology presented for scheming a variety of single molecular functional Nano machines. National academies nanotechnology testimony demands for experimentation toward molecular manufacturing. Protein catalysts designed for non-natural chemical reactions. Structural DNA nanotechnology arrays devices were designed to capture molecular structure blocks using scratch of a small protein that performed the function by natural globin proteins. Feynman Prize in Nanotechnology awarded for experimental demonstrations of mechano synthesis using AFM to control single atoms, and for computational analysis to construct complex molecular structures [4, 5].

1.2 Nanotechnology

Nanotechnology is the study of handling matter on an atomic scale and deals with developing materials holding at least one measurement from 1 to 100 range where exclusive phenomena allow innovative applications. Nanotechnology involves modeling, measuring and manipulating material by one atom or one molecule at Nano scale where Quantum_mechanical effects are important. Generally nanoscience is concerned with manufacturing improved materials and found to be very useful. At the current time nanoscience is in pre-competitive phase, still it is getting used in many industries. These Nano range materials are important in magnetic, electronics [6], biomedical [7], energy optoelectronics [8], and catalytic applications [9]. The scanning tunneling microscope (STM) about 25 years before, and four years later the atomic force microscope was invented, and that's the time when nanotechnology actually started to lift off. Scanning probe techniques primarily scanning electron microscopy have become the pillar of nanotechnology research. Based on these findings, several forms of scanning probe microscopes are important for various zones of today's research.

1.3 Bulk materials vs nanomaterials

A particle is defined as a small object that acts as an entire unit in terms of its properties, in nanotechnology. Further categorized according to size in terms of coarse particles and diameter in a range between 10,000 and 2,500 nanometers. Fine particles lie in the range of 2,500 to 100 nanometers. Nanoparticles or ultrafine particles are sized between 100 and 1 nm. A bulk material must have persistent physical properties irrespective of its size and size dependent properties are frequently perceived at the Nano regime. Consequently, the properties of materials change as their size reaches the nanoscale where quantum confinement phenomenon is witnessed and the percentage of atoms at the surface of a material becomes important and significant. Due to large surface area to volume ratio, the exciting properties of nanoparticles are observed as the percentage of atoms at the surface of material is significant in relation to the number of atoms in the bulk of the material [10].

1.3.1 Surface area to volume ratio and Quantum confinement

Nanomaterials are categorized by a large surface area to volume ratio which have a major effect on the nanoparticles properties. Consequently, a large fraction of atoms of the materials are on the surface, hence leads to surface dependent properties. The surface area to volume ration increases with the decrease in radius of the sphere and vice versa. In other words, the surface area increases when volume is distributed into smaller pieces. A greater proportion of atoms are found at the surface compared to those inside of the material. For example, 5% of atoms lie on surface of a particle of 30 nm, at 10 nm 20% of its atoms and at 3 nm 50% of its atoms lie on surface. Hence nanoparticles have a much greater surface area compared with larger components. In small nanocrystals, the electronic energy levels are not continuous like bulk but are discrete and quantized because of the confinement of the electronic wave function of the particles. This phenomenon is called quantum confinement and therefore nanocrystals are also stated as quantum dots [11, 12].

1.4 Classification of Nanomaterials

Nanoscale materials on the basis of dimensionality can be classified into four categories:

Zero dimensional structures (0-D): The materials in which all of the dimensions are less than 100nm, for e.g. length, breadth and height of a material are restricted at single point are called zero dimensional nanomaterials. It includes Nano particles, single crystal, polycrystalline and amorphous particles with all possible morphologies, such as spheres, cubes and platelets quantum dots, and composite nanoparticles.

One dimensional structures (1-D): The materials in which two of the dimensions lets say length and breadth are in the limit of nano regime having dimensions less than or equal to 100nm and one dimension is at macroscopic level are called one dimensional nanomaterial. For e.g nanotubes, nanowires, nanorods and nanofibres.

Two dimensional structures (2-D): The having one dimension (length or breadth or height) is in the limit of nano scale and other two dimensions at macroscopic level known as 2-D materials. It consists of nanofilms, nanoplates and nanobelts.

Three dimensional structures (3-D): In 3-D all of the three dimensions lie in the range of macroscopic level i.e. clusters of nanowires, nanotubes etc.

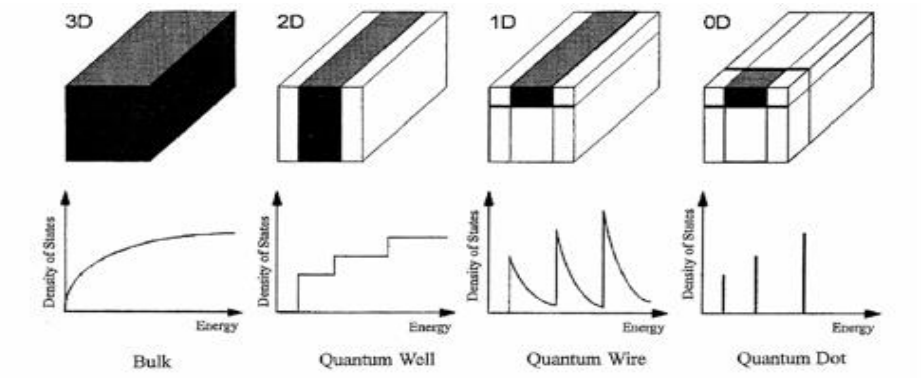

Figure 1.1: The 0-D, 1-D, 2-D and 3-D nanomaterials [13]

1.5 Properties of nanomaterials

When materials contract to Nano range, their properties will change drastically. This can be explained by the largely increased surface area to volume ratio. For example, electronic properties of many solids are transformed when they reach Nano regime.

Nanomaterials exhibits some distinct properties including electrical, magnetic, or mechanical as compared to conventional bulk particles that make the nanomaterials a relevant topic in medical, pharmaceutical and different engineering divisions. The nanomaterial owns some extraordinary and specific unusual properties which may be considerably unique from the properties of bulk materials

1.5.1 Surface Properties

The atoms present in nanomaterials have higher energy as compared to atoms present in bulk structure due to larger fraction of surface atoms. As high quantity charge species and impurities may be easily attracted to surfaces and interfaces. Surface properties of the nanoparticles and their interaction can be modified by using molecular monolayer [14].

1.5.2 Optical properties

The optical properties are the result of photon interactions with the components in semiconductor materials which gives rise to many phenomena's. Electrons in semiconductor materials can absorb photons and be excited from the valence band to the conduction band. This is called the inter band transition. The reverse of this process is called an intra band transition, occurs when electron falls from one state to another within a particular band. This is the origin for light-emitting diodes. In low-dimensional systems, electrons can be excited by photons and jump from one restrained energy level to another. These transitions are shown for a bulk material in Fig 1.2a and for a quantum structure in Fig 1.2b.

The band-to-band transition in a bulk material is mainly referred to the optical bandgap. In the case of a quantum structure, the conventional optical bandgap is no longer allowed, and the active bandgap is referred to as the transition from the ground state in the valence band to the ground state in the conduction band, as illustrated in Fig 1.2b.

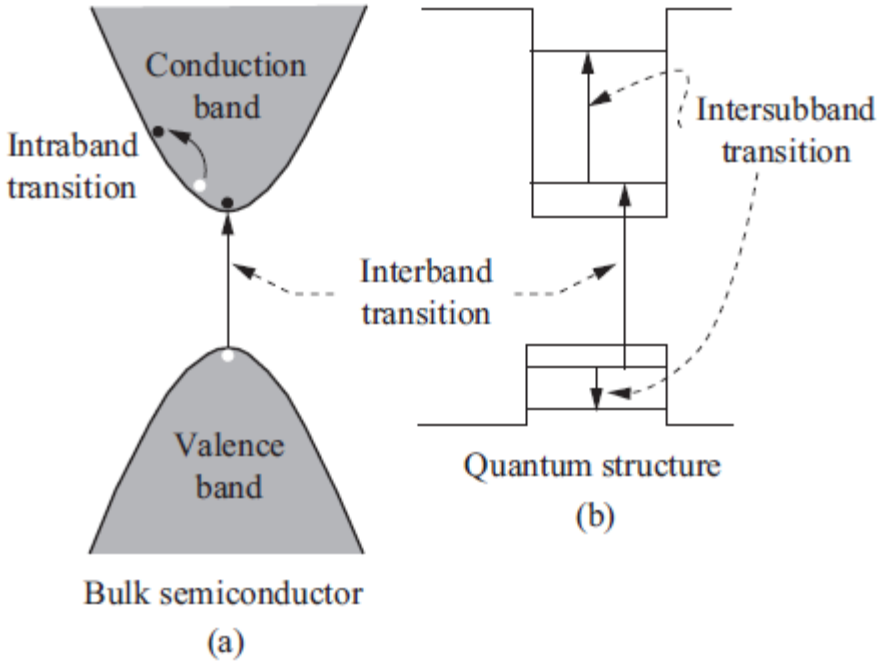

Figure1.2: Illustrations of various electronic transitions are shown for (a) a bulk semiconductor material and (b) a quantum structure

Thus, the effective bandgap in quantum structures is larger than the conventional optical bandgap in bulk materials. When the electron and hole interact with each other due to Coulomb interaction, the result is called an exciton and the exciton energy levels are typically formed in the fundamental band gap, as shown in Fig 1.3a. If the exciton is trapped by an impurity in the crystal, it is called a bound exciton or a Frenkel exciton, as shown in Fig 1.3b. The binding energy of a free exciton is generally smaller than that of a bound exciton.

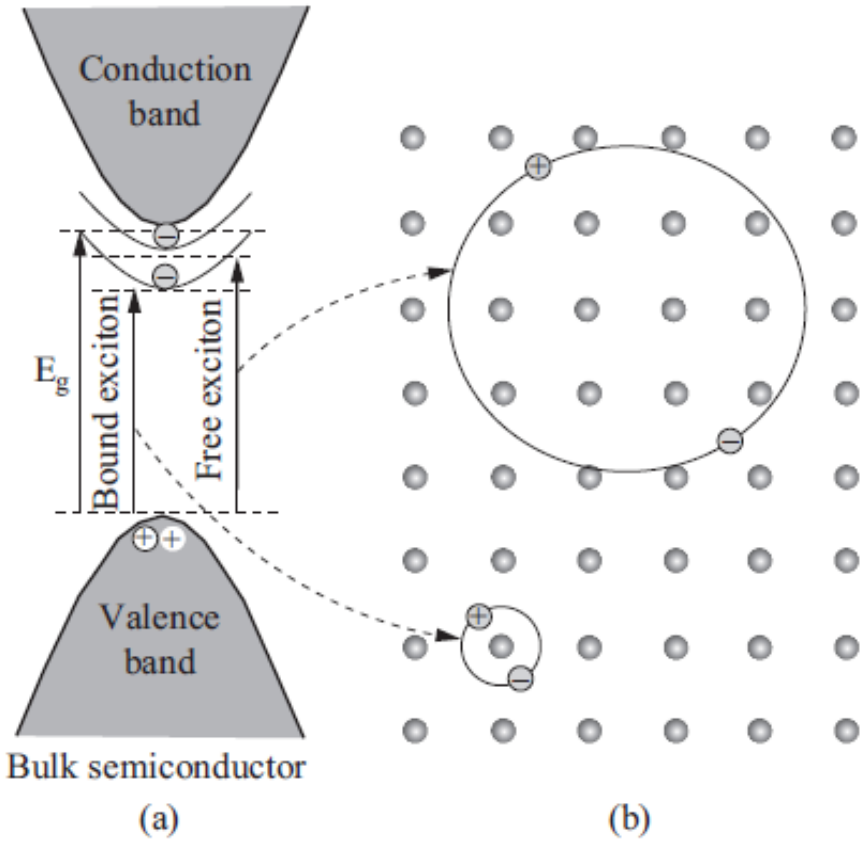

Figure 1.3: (a) A schematic presentation of excitons' energy levels with respect to the conduction band (b) The bound electron-hole pairs for both free and bound excitons [15]

Small particle sizes (~2-150nm) have high surface electron densities known as surface Plasmon. When they get excited by light at particular wavelengths and experience a collective oscillation. These oscillations are termed as a surface Plasmon resonance. The materials show different color when they are converted to nanoparticles. For example when the gold materials are changed to nanomaterials they turn into red color because for small (~30nm) monodisperse gold nanoparticles, the surface Plasmon resonance phenomena is responsible for an absorption of the blue-green portion of the spectrum (~450 nm) whereas red light (~700 nm) is reflected, generating a rich red color [16].

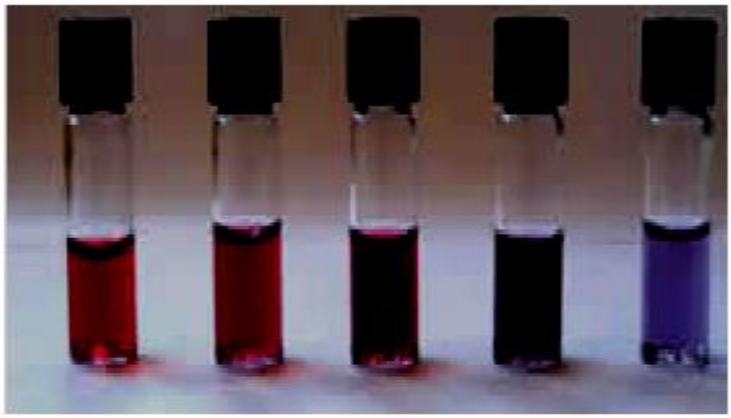

Figure 1.4: Suspensions of gold nanoparticles of various sizes [17]

1.5.3 Mechanical properties

All the nanomaterials show high mechanical strength as compared to their conventional counterparts which can be one or two times higher in magnitude than that of single crystals in the bulk form.Ccrystal perfection and reduction of defects increases as materials converts to nanoscale, which would result the improvement in mechanical strength. Cutting tools which should be harder than the material which is to be cut are made of Nano materials, such as tatalum carbide, tungsten carbide and titanium carbide. In general, hardness of metals increases linearly with increase of grain size but in case of nanomaterial, increases linearly with decrease of Particle size[18].

1.5.4 Electrical properties of the nanomaterials

In nanoparticles, 50% of all the atoms are surface atoms, therefore electric properties of these particles are no longer depends on solid state bulk phenomenon. By the reduction in the defects, electron scattering phenomenon because of crystal defects also reduced and a reduction in resistivity is practiced. On the other hand surface scattering phenomenon highly increased due to decrease in particle size is one of the main reasons for increase of the total resistivity, would result in a modified electronic structure with wide and distinct band gap [19,20].

1.6 Potential Applications of Nanomaterials

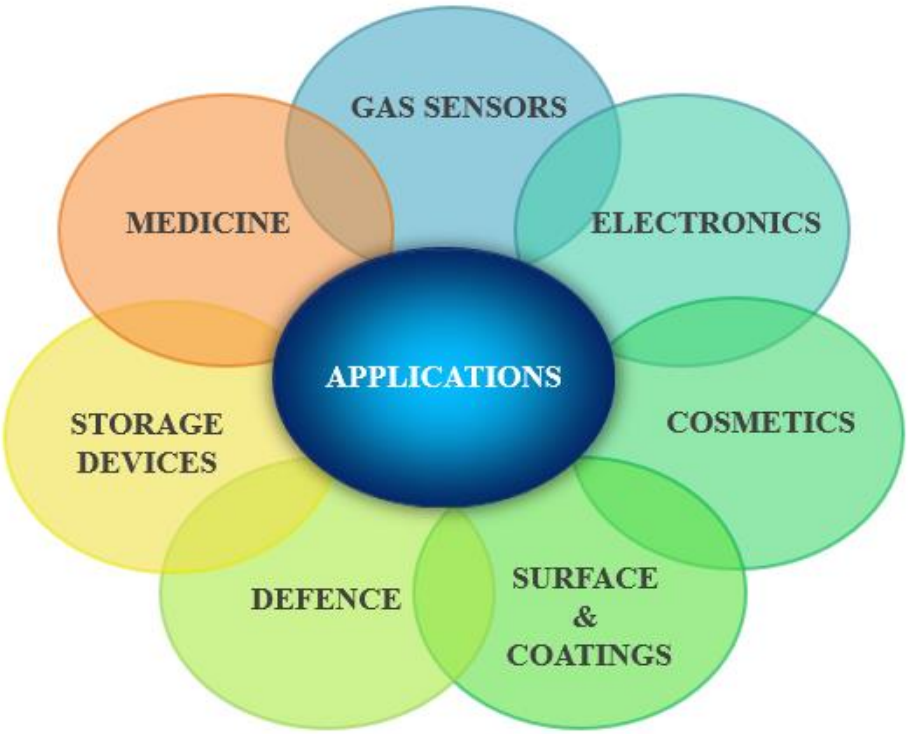

1.6.1 Medicine

Nano sensors enable drugs to be transported to the right location in the body by attaching the drug to Nano sized carrier then they become confined at the disease site i.e. cancer. Finally they release medicine that kills the tumor [21].

1.6.2 Electronics

Electrodes made from nanowires allow flat panel displays to be flexible and thinner than the old ones. The silicon transistors may be swapped by transistors based on Carbon Nanotubes. Nano rods is an upcoming technology in the displays technologies due to less intake of electricity and reduced heat emission. Size of are reduced to greater extend as microprocessors chips produced

before were between 65nm to 45nm. Later with the help of nanotechnology 22nm chips were made [22].

1.6.3 Defense

By using nanotechnology military would be capable to create sensor systems that could sense biological species-. Nanomaterials can be injected in the material on the soldier uniforms to protect soldiers from many various dangers such as chemicals and high temperatures.

1.6.4 Storage devices

Nano-scale synthesized magnetic materials also have applications in data storage, such as storage capacity of computer hard disks is increased with magnetic nanomaterials. Current research shows that 1000 GB of memory can fit on the head of the pin by means of nanotechnology.

1.6.5 Nano sensors

Nano robots of 1.5 nm across are proficient of calculating particular molecules in chemical sample. Capable of replication using environmental resources and detect toxic components in environment.

1.6.6 Cosmetics

Nanomaterials such as Nano pigments are used in skin creams and oral hygiene products. TiO_2 and ZnO are used in Sunscreens because they are known to reflect and scatter UV light which protect skin from adverse effects of UV light including skin cancers and recent studies shows that if TiO_2 Nano pigments enters into blood stream, no adverse effects are perceived [23].

1.6.7 Surface and coatings

Engineered nanofibers are used to make clothes, water and stain repulsive or wrinkle free using Nano sized whiskers that made water to bead up on the surface. Nanotechnology has been used to integrate tiny carbon particles and assure full surface protection for the electrostatic charges for the wearer. Nano ceramics particles have enriched the heat resistance and smoothness of common house hold equipment such as the flat iron. Textiles with Nano technological finish can be washed less repeatedly and at lower temperatures. Also used to fabricate spill and dirt resistant, antibacterial fabrics [24].

CHAPTER 2

LITERATURE SURVEY

2.1 Spinel Ferrites

In this review, the focus will be on spinel ferrites nanocrystals because they are observed as two of the most important inorganic nanomaterials due to their electronic, optical, electrical, and gas sensing properties. Among the magnetic materials that have wide range of practical applications in nanotechnology. They are extensively used in high frequency applications, because an AC field does not induce unwanted eddy currents in an insulating material [25, 26]. Ferrites have three diverse structural symmetries garnet, hexagonal and cubic which can be determined by the size and charge of the metal ions that balance the charge of the oxygen ions[27]

The spinel ferrite structure $MeFe_2O_4$, where Me refers to the metal, can be described as a cubic close-packed arrangement of oxygen atoms, with Me^{2+} and Fe^{3+} at two different crystallographic sites. These sites have tetrahedral and octahedral oxygen coordination (termed as A and B-sites, respectively), so the resulting local symmetries of both sites are different (Fig. 4). The spinel structure contains two cation sites for metal cation occupancy. There are 8 A-sites in which the metal cations are tetrahedrally coordinated with oxygen, and 16 B-sites which possess octahedral coordination. When the A-sites are occupied by Me^{2+} cations and the B-sites are occupied by Fe^{3+} cations, the ferrite is called a normal spinel. If the A-sites are completely occupied by Fe^{3+} cations and the B-sites are randomly occupied by Me^{2+} and Fe^{3+} cations, the structure is referred to as an inverse spinel. In most spinel's, the cation distribution possesses an intermediate degree of inversion where both sites contain a fraction of the Me^{2+} and Fe^{3+} cations. Magnetically, spinel ferrites display ferrimagnetic ordering. The magnetic moments of cations in the A and B-sites are aligned parallel with respect to one another. Between the A and B-sites the arrangement is antiparallel and as there are twice as many B-sites as A-sites, there is a net moment of spins yielding ferrimagnetic ordering for the crystal.

2.1.1 Structural symmetries of Spinel Ferrites

The spinel ferrite structure can be described as a close-packed arrangement of oxygen atoms and contains two cation sites for tetrahedral and octahedral coordination, therefore the consequent instinctive symmetries of both sites are diverse (Fig. 4). In most spinel's, the cation distribution possesses transitional degree of reversal and their magnetic moments are aligned antiparallel with each other. Magnetically, spinel ferrites are ferrimagnetic in nature. There is a net moment of spins yielding ferrimagnetic ordering for the crystal between both sites. The choice of metal cation and the distribution of ions between the A and B-sites, offer a tunable magnetic system [29].

Materials which crystallize in the spinel structure have the general formula AB_2O_4 in which A and B show tetrahedral and octahedral cation sites, and O indicates the oxygen anion site (Figure 2.1). Spinel ferrites with the general formula $MeFe_2O_4$,where Me signifies a divalent cation such as Mn, Zn, Co, Ni, Cu, , Cd, or Mg and Fe is the trivalent iron cation, have the same crystallographic structure as the mineral spinel ($MgAl_2O_4$)[30,31]. The oxygen anions form the close face-centered cube (FCC) structure consist of 64 tetrahedral (A) and 32 octahedral (B) empty spaces partly populated by Fe^{3+} and Me^{2+} cations [32]. This type of spinel ferrite are schematically illustrated in Figure

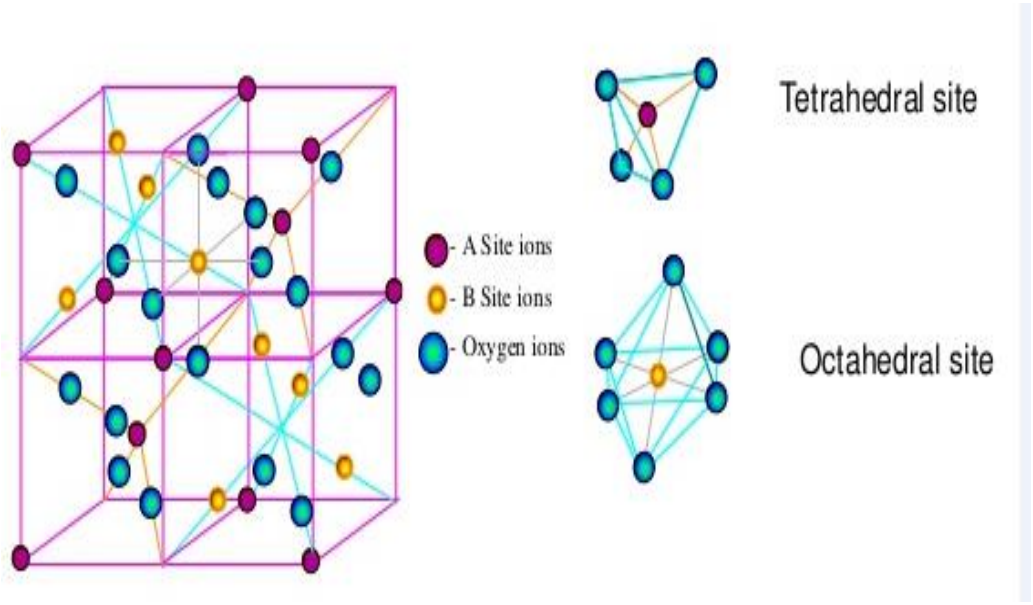

Figure 2.1: Schematic of a partial unit cell and ferrimagnetic ordering of spinel ferrite structure [28].

2.2 Classification of ferrites

Ferrites are divided into two types, soft and hard ferrites, based on their aptitude to be magnetized and demagnetized. Soft materials are easy to magnetize and demagnetize, so can be used for electromagnets, whereas hard materials are used for permanent magnets because of their high coercivity[33]. Table 2 gives a qualified description of both types of ferrites. Hard ferrite magnets are further classified in two magnetic forms isotropic and oriented. Isotropic magnets are formed to preferred shapes, sintered and then magnetized which exhibit a diffident magnetic field and have applications in ring magnets and cycle turbines. Oriented magnets are designed to form under a strong magnetic field and then sintered. These oriented magnets displayed a very strong magnetic field and used in magnets of two wheelers like bikes, loudspeakers etc. [34]. Soft ferrites are ceramic electromagnetic materials, very hard and stiff and found in black or dark gray color. Soft ferrites are also semiconductors, implying, they are anywhere between insulators and conductors based on their ability to conduct electron flow through the material. The general properties and applications of hard and soft magnetic materials are given in Table 2.1.

Soft magnetic	Hard magnetic
High saturation magnetization (1–2*T*)	High saturation magnetization (0.3–1.6*T*)
Low coercivity (H_c)	High coercivity
High permeability	Not important, but low
Low anisotropy	High anisotropy
Low magnetostriction	Not important
High Curie temperature (T_c)	High T_c
Low losses	High-energy product
High electrical resistivity	Not important

Table 2.1: General properties and applications of hard and soft magnetic materials

2.3 Advantage over other magnetic materials

High permeability stability are important characteristics, which have extended the practice of ferrites into high frequency, filter circuits, adjustable inductors and other high-frequency electronic devices. Ferrites have many advantages over other electromagnetic materials including low eddy current losses over extensive frequency series because of their high resistivity and high stability over a wide range of temperature. Whereas other magnetic materials and metallic alloys have low electrical resistivity that makes them useless for applications at high frequencies because they allow induced or eddy currents to flow within the materials themselves, thus producing heat. Therefore, the material become inefficient at higher frequencies. Another significant feature in selecting ferrites is that they are normally inexpensive than magnetic metals and alloys.

2.4 Literature review of spinel ferrite as gas sensors

Spinel type ferrites are very multipurpose gas sensing materials with sustained development and show larger industrial applications. Ferrites can suggest high sensitivity, selectivity, and long-term stability. Though, the properties of ferrite gas sensors are still not completely understood, hence required further expansion and growth. Gas detection is based on variability of electrical, optical, mass or electric properties of the material and attracting the most interest because of simple, fast and less expensive mechanism [35]. The most common gas sensors are centered on single crystalline or polycrystalline metal oxide semiconductors [36], carbons [37], carbon polymer composites [38] and conducting polymers [39]. For n-type semiconductors, the resistance decreases after exposure to various gases and for p-type oxide semiconductor, an opposite change in the electrical resistance is projected [40].

In spite of the large diversity of existing oxide based gas sensors, researchers continue to search for more effective gas sensor materials with high sensitivity and fast response time to detect gases at lower temperatures. Spinel ferrites with AB_2O_4 formula unit are very favorable complex oxides for gas sensing applications [41]. Metal oxide semiconductor gas sensor materials have been intensively examined since Seiyama et al. first projected in 1962 about the gas sensing properties of semiconducting thin films. A higher gas response stability follows in post-transition metal

oxides with a filled d^{10} shell form oxides , d^{10} oxides are the most stable and sensitive gas sensing materials, subsequently they can be reduced by varying the d^{10} cation electron configuration. Gas sensing properties of other spinel oxide compounds such as stannates, aluminates, cobaltite's, and manganite's have also been studied. Yet spinel ferrites are the most broadly explored for gas sensor applications [42].

Gas sensing plays an important role for a range of various necessities including detection of explosive gases, environmental protection, and to detect combustible gases. The global gas sensor market was about 1.7 billion USD in 2012 and is estimated to develop for the next six years at an annual growth rate of 5.1%.

2.5 Gas sensing mechanism in spinel ferrites

Spinel ferrite gas sensors operate according to the well-known semiconductor gas sensing mechanism [43]. Oxygen species chemisorb onto metal oxide particles surface by trapping electrons (Fig 2.2), which produces a resistance layer due to electron depleted space charge on the conducting layer. When gas molecules react with chemisorbed oxygen, electrons are released back to oxide according to the following reaction: $CO + O^{-}_{ads} \rightarrow CO_2 + e^{-}$. The release of electrons changes conductivity in the space charge layer. A denser space charge layer increases the sensitivity. Subsequently, the smaller particle size is advantageous for a higher gas response, because the volume of space charge layer is analogous to volume of gas sensing particle.

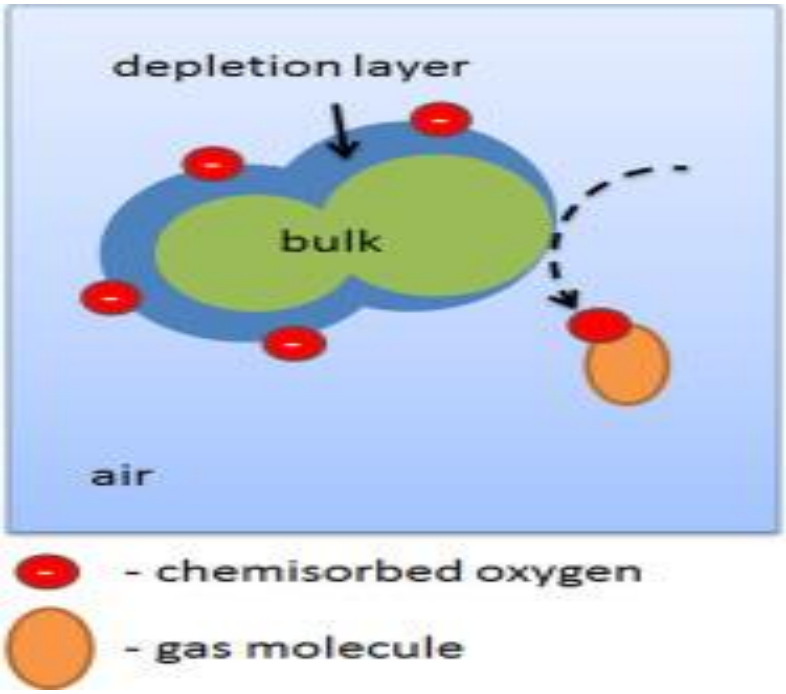

Figure 2.2: Schematic of gas sensing mechanism semiconductor oxide gas sensors [44]

2.5.1 N-type spinel ferrite gas sensors

Charge carrier transport in n-type spinel ferrites is delivered by conductivity of e^- between iron cations positioned at octahedral sites. A greater concentration of Fe^{2+} increases e^- conductivity ($Fe^{3+} + e^- \leftrightarrow Fe^{2+}$). After chemisorption of oxygen species on the surface of spinel ferrite, Fe^{2+} is oxidized to Fe^{3+}. And e^- are released back when oxygen reacts with exposed gas, and Fe^{3+} is reduced to Fe^{2+}, therefore increasing the amount of Fe^{3+} and Fe^{2+} pairs and inclusive electrical conductivity. The oxidation–reduction reaction on the surface of n-type spinel ferrite surface is reversible as confirmed by others. Most popular examples of n-type spinel ferrite gas sensors are $ZnFe_2O_4$, $MgFe_2O_4$and $CdFe_2O_4$.

2.5.2 P-type spinel ferrite gas sensors

P-type spinel ferrites are normally inverse spinel structure ferrites with Me^{2+}cations in octahedral beside Fe^{3+}. The p-type conductivity arises from hole hopping between Ni^{2+} and Ni^{3+} in octahedral sites ($Ni^{2+} + h^+ \leftrightarrow Ni^{3+}$). A common p-type spinel ferrite is $NiFe_2O_4$. Higher chemisorbed oxygen concentrations will lead to an improved gas response [45]

CHAPTER 3
EXPERIMENTAL SETUP AND MEASUREMENTS

3.1 Experimental methods of fabrication

Synthesis methods show very significant importance to regulate the size and surface area of nanomaterials. There are two approaches for engineering the nanomaterials:

3.1.1 Top down

The top-down approach includes carved down the size of materials from the macroscopic to the nanometer scale which generally relies on the chemical or thermal processes for their fabrication.

3.1.2 Bottom up

In the bottom-up approach, single atoms or molecules are assembled into larger nanostructures, guarantees the best control over all particles in the system. This is a very dominant process of producing indistinguishable structures with atomic accuracy, and are still much simpler than nature's complex structures. This approach allows control of the structural and chemical design however, manual assembly of individual nanometer sized modules is clearly exorbitant in cost and time [46].

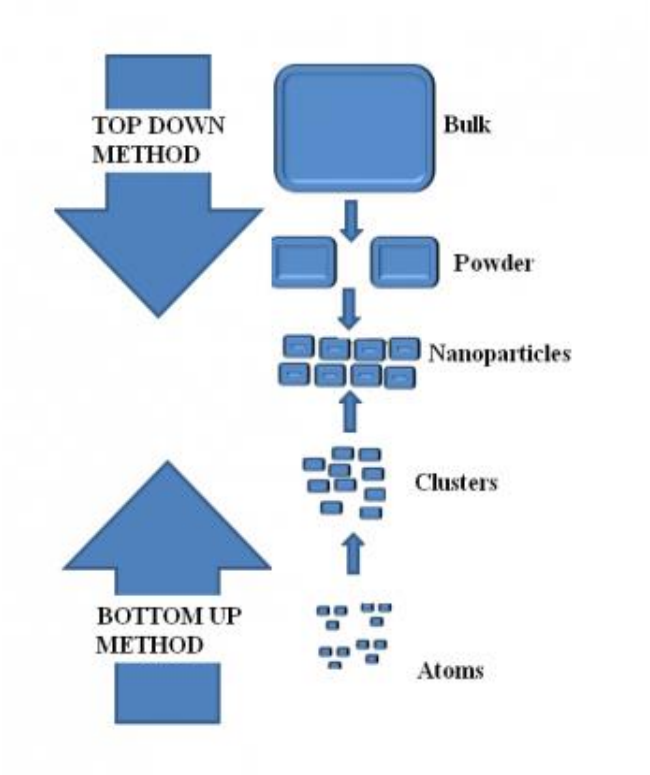

Fig 3.1: Schematic diagram of various approaches for preparing nanoparticles [47].

3.2 Synthesis of Nano ferrites by various techniques

- Chemical Vapour Deposition [48]
- Sol–gel process [49]
- Hydrothermal method [50]
- Microemulsion technique [51]
- Co-precipitation method

3.2.1 Co-precipitation method

The process is described in the following brief overview:

- Desired products are generally sparingly soluble in a certain solvent.
- Supersaturation occurs over time which is a deterministic factor in the growth of the products.

- High supersaturation leads to nucleation to form a large number of clusters or nuclei.
- Secondary growth processes such as Ostwald ripening or aggregation can dramatically affect the size and morphology of the final product.
- The precipitates are then washed and filtered several times to maintain PH.
- The dried sample is further ground to form a homogenous powder.

3.2.1.1 Ostwald ripening in co-precipitation

The molecules on the surface of a particle are less stable than the ones in the inside i.e. in a cubic crystal of atoms, all the atoms inside are bonded to 6 neighbors and are more stable than the atoms on the surface which are only bonded to 5 neighbors or less, as the system tries to lower its overall energy, molecules on the surface of a small particle will incline to separate from the particle and diffuse into the solution. Results in increase the concentration of free atoms in solution. Free atoms in solution become supersaturated and therefore, all the smaller particles will shrink and larger particles will grow in size. After some time, the entire population of particles will become one enormous spherical particle to minimize the total surface area [52].

Method	Reaction temp. (°C)	Reaction period	Particle size (nm)	Size distribution	Specific surface area	Yield
Sol–gel auto combustion	550–1100	Hours	>25	Relatively wide	Medium	Very high
Co-precipitation	20–90	Minutes	<25	Relatively narrow	High	High
Hydrothermal	105–270	Days	<25	Narrow (controllable)	High	Medium

Table 3.1: Comparison of different synthesis methods

3.3 Experimental method to be adopted

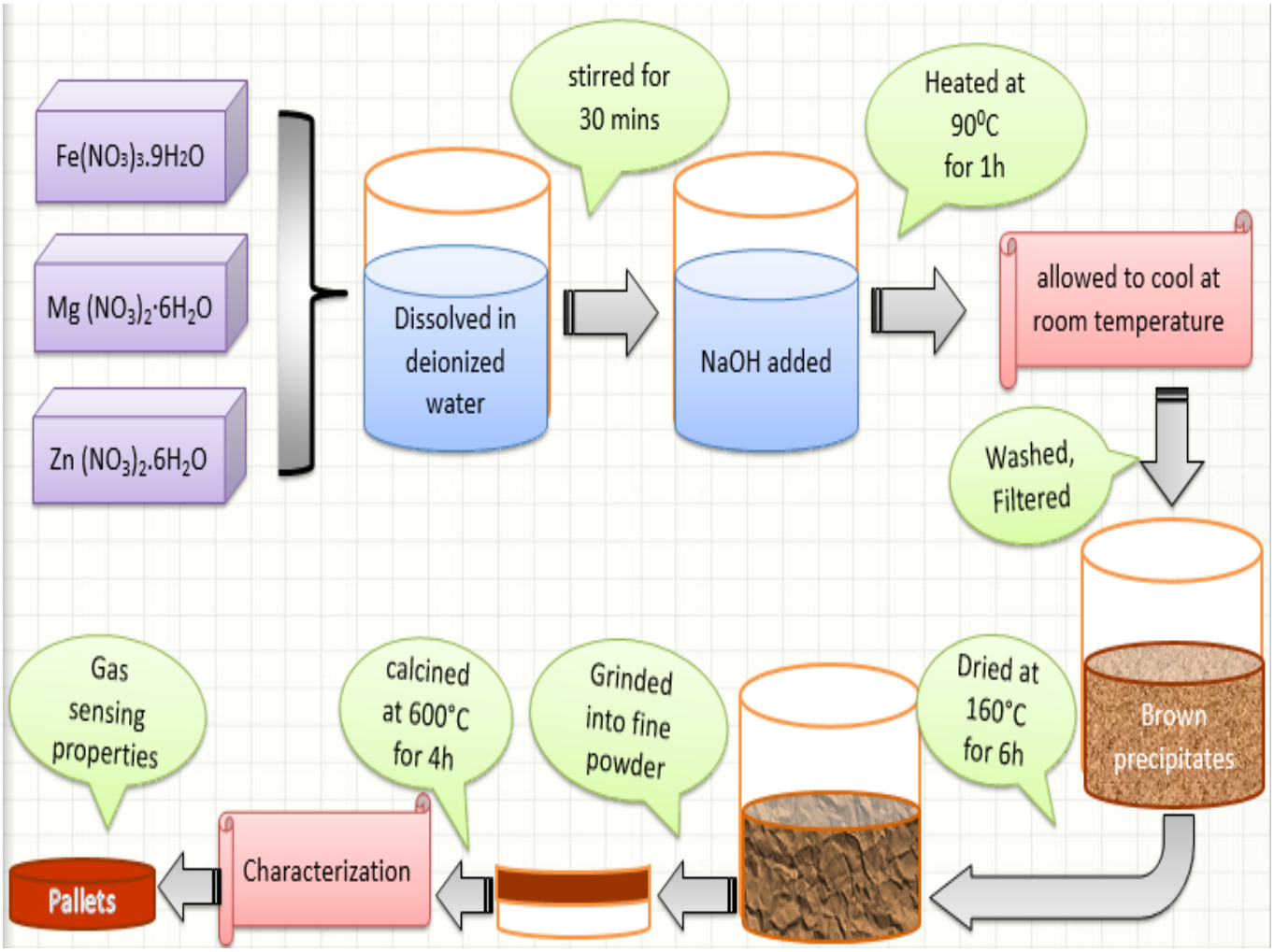

3.3.1: Apparatus

For the synthesis of Mg-Zn ferrite nanoparticles the following apparatus was used

• Digital Balance

• Hot Plate

• PH meter

• Mortar and Pestle

• Die

• Hydraulic Press

• Crucible

• Oven

• Furnace

3.3.2: Theory of the operation

Powders of $Mg_{1-x}Zn_xFe_2O_4$ (x=0.0, 0.2, 0.35, 0.5) were synthesized by co-precipitation method. This process is a convenient, environment friendly, inexpensive, high-yielding, low cost and facile synthesis method for the preparation of spinel ferrite nanomaterials, which included the following procedure. A.R. grade Fe $(NO_3)_3 \cdot 9H_2O$ provided by EMSURE® Merck KGaA -Darmstadt Germany (99% purity), Mg $(NO_3)_2 \cdot 6H_2O$ and Zn $(NO_3)_2.6H_2O$ were dissolved in an appropriate proportion and stirred for 30 mins then heated at 90^0C. Simultaneously stirred NaOH delivered by Fischer Chemical Ltd was added to ferrite solution and heated for 1h. The solution is then allowed to cool at room temperature. The precipitates were filtered and washed repetitively with deionized water and dried at 160°C for 6h. The dried material was grinded into fine powder and calcined at 600°C for 4h in tabular furnace. The whole procedure was repeated four times for synthesis of $Mg_{1-x}Zn_xFe_2O_4$ (x=0.0, 0.2, 0.35, 0.5) samples. X-ray diffraction patterns were obtained using X-ray diffractometer (STOE GERMANY Theta-Theta) with generator voltage of 40 KV, current 40mA and Cu Kα radiation (λ= 1.5406 Å). Fourier Transform Infrared Spectral (FTIR) analysis was done by Perklin Elmer Spectrum FTIR spectrometer to ratify the presence of metal-oxygen vibrations bands in $Mg_{1-x}Zn_xFe_2O_4$ nanoparticles. JEOL JSM-6390 scanning electron microscopy (SEM) was used to record microstructures. The dielectric properties have been investigated using Wayne Kerr LCR 6500B. Optical properties were studied using UV-Visible spectroscopy of model (UV-2800) in the wavelength range of 300 to 1000nm. The homogenized powder was then compacted into pellets of about ~3 mm thickness and 13 mm diameter, at a pressure of 5 tons for

4 mins. Further these pallets were used for dielectric and gas sensing measurements.

3.4 Characterization techniques

Herein we have described the techniques used for the characterization of prepared nanomaterials.

3.4.1 Structural Characterization

X-ray diffraction (XRD) is a flexible and useful technique for analyzing the detailed information about crystallographic structure of the Nano materials. Powder samples are examined as in random orientations to assure that all crystallographic directions are tested by the monochromatic x-rays beam and used to define inter planar spacing of the unknown material. Schematic of Bragg condition is shown in Figure. X-ray diffraction patterns were obtained using X-ray diffractometer (STOE GERMANY Theta-Theta).

Figure 3.2a: X-ray diffractometer (STOE GERMANY Theta-Theta)

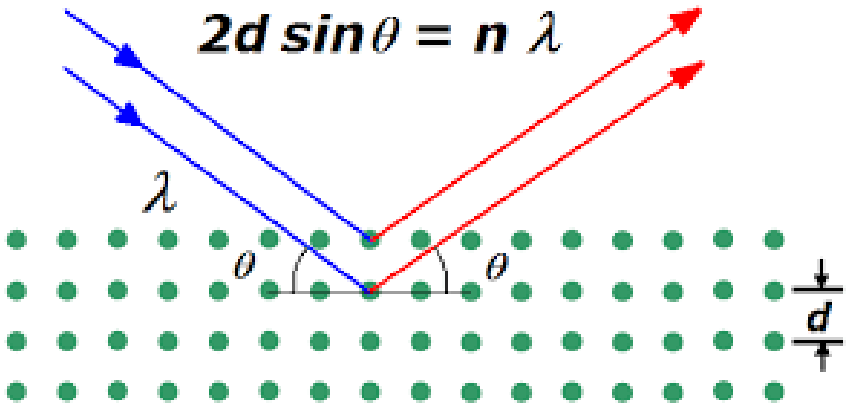

Figure 3.2b: Schematic of X-ray diffraction technique (Bragg's law) [53].

The crystallite size (D) of the material can be assessed using Debye Scherer's equation given as:

$$D = \frac{0.9\lambda}{\beta\cos\theta}$$

Where K is Scherrer‟s constant, λ is wavelength of X-ray, β is full width at half maximum value (FWHM) in radians and θ is the diffraction angle. XRD densities (ρ_{xrd}) of the prepared samples can be calculated by the formula:

$$\rho_{xrd} = \frac{8M}{N_A a^3}$$

$\boldsymbol{\rho_x}$ is the density calculated from XRD data, M is the molecular weight, $\mathbf{N_A}$ is the Avogadro's constant, and **a** is the lattice constant of the cubic unit cell.

Further, porosity P of the samples can be determined using relation:

$$P = 1 - \frac{\rho_m}{\rho_x}$$

Where ρ_m and ρ_x are the mass and x-ray densities.

3.4.2 Surface Morphological Characterization

Scanning electron microscope is deliberated to be a vital for micro structural analysis. It illustrates the morphology, compositional differences, and crystal orientation of samples. SEM consists of electron gun, condenser lens, apertures, deflecting coils and objective lens. When a beam of electrons impinges on a solid surface, it undergoes several interactions at the surface. The incident electrons are transmitted, absorbed or reflected (Figure 1.12 (a)). The ougoing beams from the sample consist of electrons, X-rays, or visible-IR photons and each of these signals contains information about the surface conditions, structural compositions and impurity contents of the material [54].

Figure 3.3a: JEOL JSM-6390 scanning electron microscopy (SEM)

Secondary Electrons

When the incident beam electrons hits a sample atom electrons, ionizes the atoms and knock it out of its outermost shell. These are the secondary electrons. Secondary imaging mode reveals the information about the surface topography.

Backscattered Electrons

When the incident beam strikes with the nucleus of the sample atom backscattered electrons are produced. Backscattered electrons are related to the atomic number and density of the sample surface. A sample surface with greater atomic weight area scatters more backscattered electrons as compare to the low atomic weight area[55]..

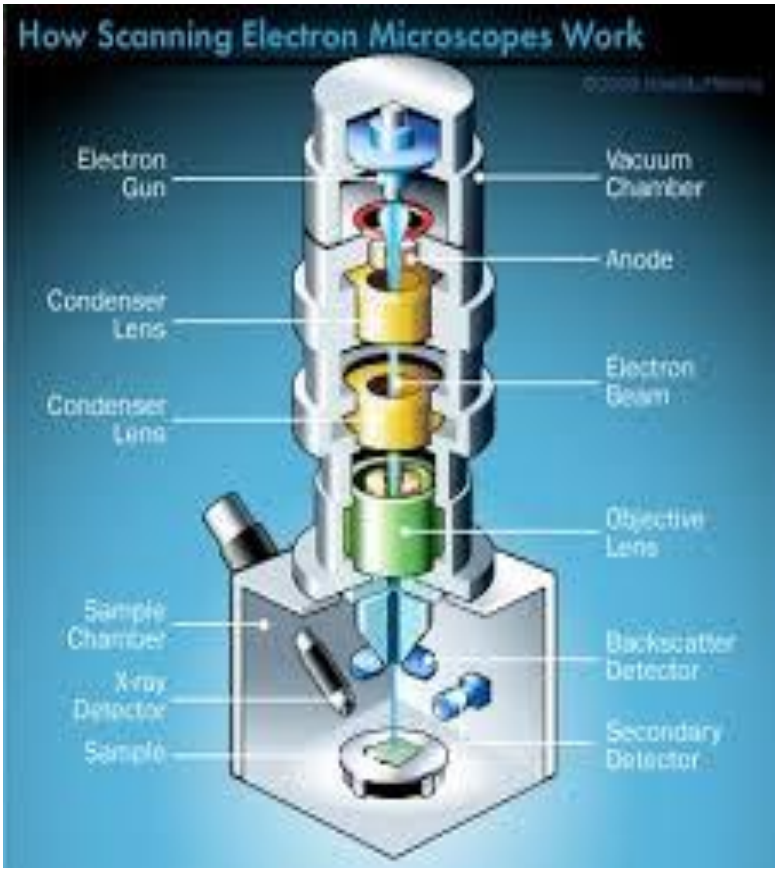

Figure 3.3b: Schematic diagram for SEM [56]

3.4.3 Fourier Transform Infrared Spectroscopy (FT-IR)

Fourier transform Infrared Spectroscopy is a common technique to reveal the vibrations of metal-oxygen bonds. In general, FT-IR spectroscopy is used to measure that how well a sample absorbs

or transmits light at each wavelength. Therefore, this system is able to give information of the chemical bonds in a material. Fourier Transform Infrared Spectral (FTIR) analysis was done by Perklin Elmer Spectrum FTIR spectrometer to ratify the presence of metal-oxygen vibrations bands in $Mg_{1-x}Zn_xFe_2O_4$ nanoparticles. In FT-IR analysis there are three commonly examined pieces of data the peak position, the peak width, and the peak intensity. The peak position is commonly used for the identification of materials.

Figure 3.4a: Perklin Elmer Spectrum FTIR spectrometer

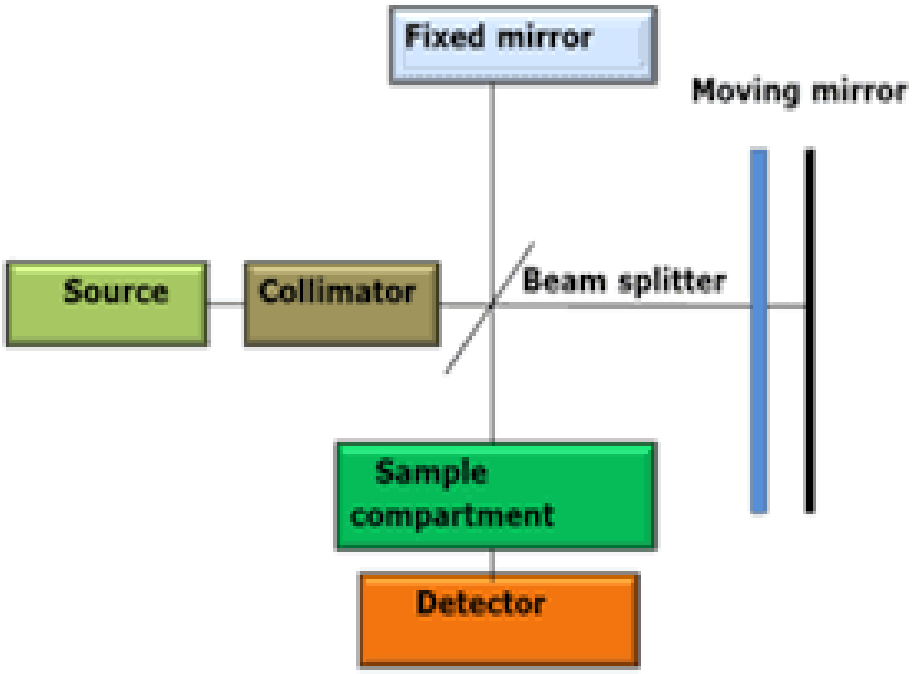

Figure 3.4b: Schematic of FT-IR spectrometer [57]

Working

It works on the principle of the optical instrument interferometer. It consists of three components fixed and movable mirror and beam splitter. Fixed mirror has fixed length and movable mirror has changing lengths so that two beams can interfere each other. Half of the beams are reflected off towards the fixed mirror and half is transmitted towards the movable mirror through a beam splitter. A light is then recombined by two mirrors and drive back to the beam splitter. A signal is generated after interference and is called interferogram. A signal from interferogram is encoded with the information about every infrared frequency from source [58].

3.4.4 UV-visible Spectroscopy Ultraviolet-visible spectroscopy

The main parts of a spectrophotometer are a light source (usually Tungsten filament (300-2500 nm)), a monochromator, a holder and a detector which is typically a photodiode, which filters the light so that light of a single wavelength reaches to the detector [59]. Ultraviolet-visible spectroscopy refers to absorption spectroscopy in the visible and near UV and IR regions. In this region, molecules experience electronic transitions. UV/vis spectrophotometer measures the intensity of light passing through a sample (I), and associates it to the intensity of light before it passes through the sample (Io) and absorbance is given as:

$$A = \log_{10}(I_o / I)$$

The ratio I / Io is called the transmittance, and is usually expressed as a percentage (% T).

$$A = -\log (T/100)$$

Figure 3.5a: UV-Visible spectroscopy of model (UV-2800)

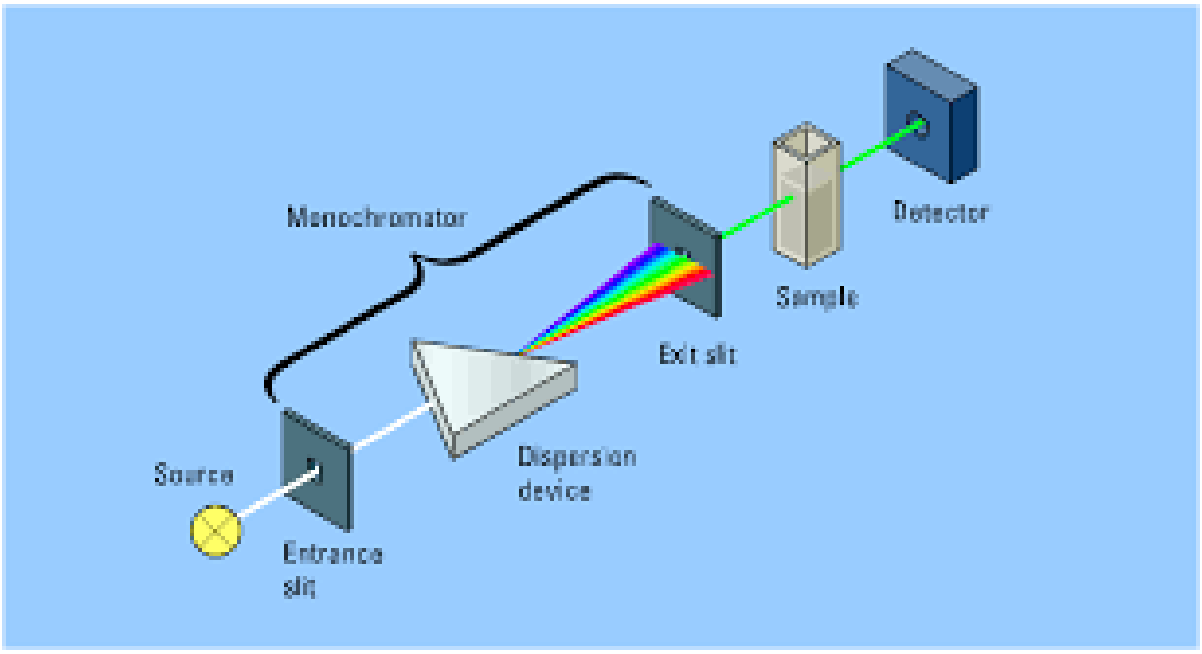

Figure 3.5b: Ray diagram of UV-visible spectrometer

3.4.5 DIELECTRIC CHARACTERIZATION

LCR meter is used for dielectric measurements, which is an electronic device that is used for the measurement of inductance, capacitance and resistance with high precision. This device has capability to proceeds the measurements of samples with variable circuit arrangements and by adjusting the frequency range according to requirements.

Figure 3.6: Wayne Kerr LCR 6500

Generally there are two kinds of methods used in LCR meter.

- Current voltage measurement Technique
- Bridge Technique

Current voltage method

This technique is used for the high frequency range applications. In this technique by finding the current and voltage values impedance of DUT can be found. Further with the different arrangements of circuit's low impedance and high impedance measurements are also possible.

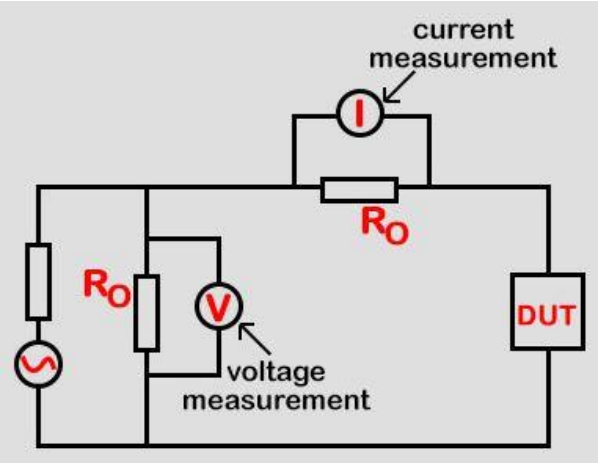

Figure 3.7a: Circuit diagram for High impedance

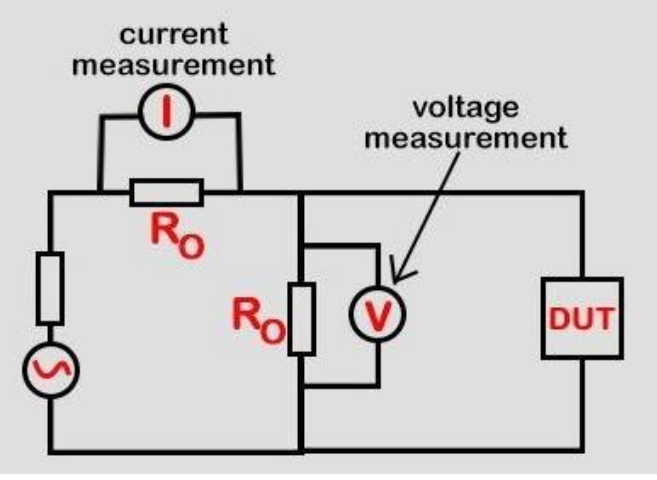

Figure 3.7b: Circuit diagram for Low impedance [61]

Bridge Technique

In LCR meter bridge technique is only applicable for low frequency range study. Measurements of samples can be taken below frequency range of 100 kHz. Bridge method is based on Wheatstone bridge principle. In Wheatstone bridge circuit the device under test (DUT) is placed in it its impedance is denoted by Zu. The other impedances Z2 and Z3 are known. Impedance Z1 changes until current stop flowing through device. At this balance position the impedance of unknown can be measured by using the given below equation.

Z1/Zu=Z2/Z3

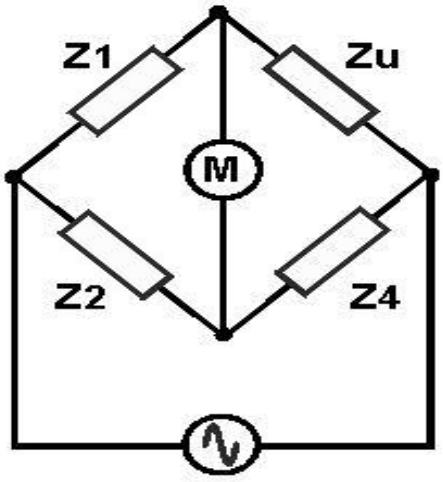

Figure 3.8: Circuit diagram for Bridge Technique [62]

3.4.5 Gas sensing characterization

Gas Sensing Setup

A specially designed gas sensing system was used for sensing of various gases. This sensing setup is consisted of a vessel with two input and output valves. The pallet sensor was placed into the measuring chamber and outputs were connected to a Keithley Multimeter. Commercially available gases of 99% purity were used to study the sensing response. The required gas was injecting by

syringe into the system through a valve provided on a vertical wall of the closed system. Constant voltage was applied to the sensors, and current was measured by a digital ammeter and from the measured current, resistance is calculated as a function of time at constant temperature both in air and in the presence of the gas [63]. The detail of gas sensing set-up well as measurement protocol has been demonstrated elsewhere [64-67]. Before the beginning of a new measurement, the sensor element was submitted to a heat treatment at 100°C for 10 minutes to form the initial structure and to attain its thermodynamic stabilization. Heat cleaning of the samples was found to be essential for improved and reproducible sensitivity [68]. Finally, the sensitivity is calculated by using following relation:

$S = \frac{\Delta R}{Ra} = \frac{|Ra-Rg|}{Ra}$, Where Ra is the sensor resistance in the air and Rg is the sensor resistance in the presence of test gas.

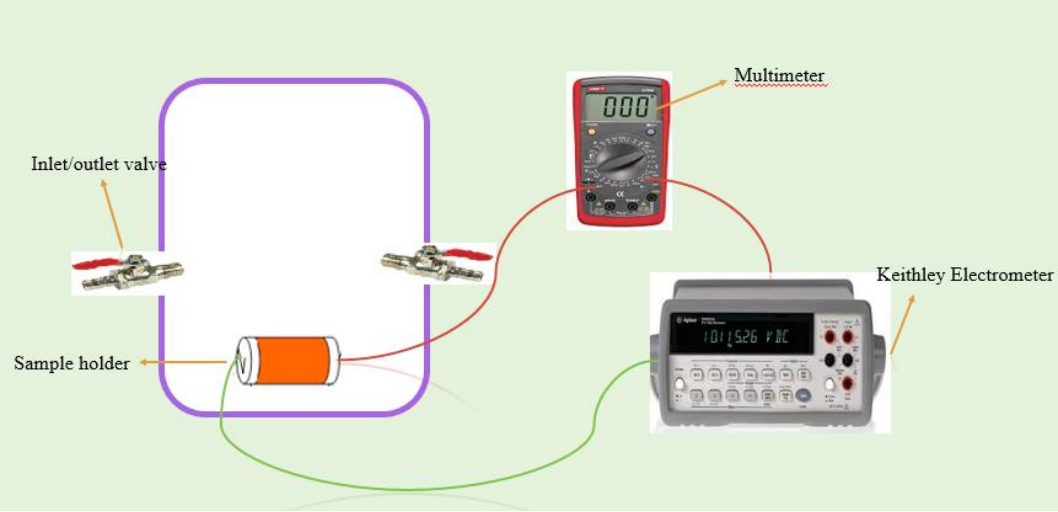

Figure 3.9: Gas sensing setup

Mechanism

The detection mechanism of these ferrite materials is based on the property of changing the resistance of the sensing material in the presence of a determinate gas. A porous structure favors the gas molecules to enter easier into the material. In the former case, the atmospheric oxygen adsorbs on the surface by extracting electrons from the conduction band to form super oxides or peroxides. Then the exposed gas molecules captures the lattice oxygen from the surface of the

sample at room temperature. This would result the oxygen deficiency in the bulk of the material preferably at the surface. Upon exposure to the gas, it reacts with the adsorbed oxygen, releasing the trapped electron to the conduction band and subsequently lowering the resistance. Sensors work on the principle of change in resistance due to the adsorption of gases [69]

The gas-sensing mechanism of ferrites is based on the surface-controlled process. The surface-controlled process for oxide semiconductor gas sensing materials can generally be described as follows [70] The adsorption and ionization of oxygen from air containing the test gases can be expressed as:

$O_{2gas} \longrightarrow O_{2ad}$

$O_{2ad} + e^- \longrightarrow 2O^-_{ad}$

$O^-_{ad} + e^- \longrightarrow O^{2-}_{ad}$

Where the subscripts 'gas' and 'ad' indicate the gaseous and oxygen adsorbed oxygen, respectively. The reducing gases adsorbed on the surface of the sensor materials and their action between the adsorbed gas and the adsorbed oxygen species is for example, O^-_{ad} and O^{2-}_{ad} will then proceed as:

$R \longrightarrow R_{ad}$

$R_{ad} + O^-_{ad} \longrightarrow RO_{ad} + e^-$

$R_{ad} + O^{2-}_{ad} \longrightarrow RO_{ad} + 2e^-$

Finally, desorption of the resulting product will take place as

$RO_{ad} \longrightarrow R_{gas}$

The adsorption of the gas depends on the type of the test gas and the sensor material which affect the sensitivity and response time. The gas sensing property of different gases is due to difference in the adsorption and reaction process. The amount of absorbed oxygen species is quite important for providing enough reactants for the reactions [71]

CHAPTER 4

RESULTS, ANALYSIS AND DISCUSSION

4.1 XRD Analysis of Prepared Zn substituted Mg ferrites

Structural properties of prepared samples were obtained by using X-ray diffraction technique. In XRD Cu Kα X-rays of wavelength λ = 1.5406A^o was used for the analysis of the prepared samples -and scanned in 2θ ranges from 20^{o}C to 90^{o}C. In first step indexing of the diffraction pattern is done and the Miller indices to each plane were assigned. Strong Bragg reflections corresponds to the planes (220), (311), (400), (422), (511), (440), (533) and (622) as shown in Fig 4.1. The peak intensity (311) was relatively higher than others. The higher intensity can be attributed to an annealing effect that boosts the crystallinity and specific orientation of the crystallites.

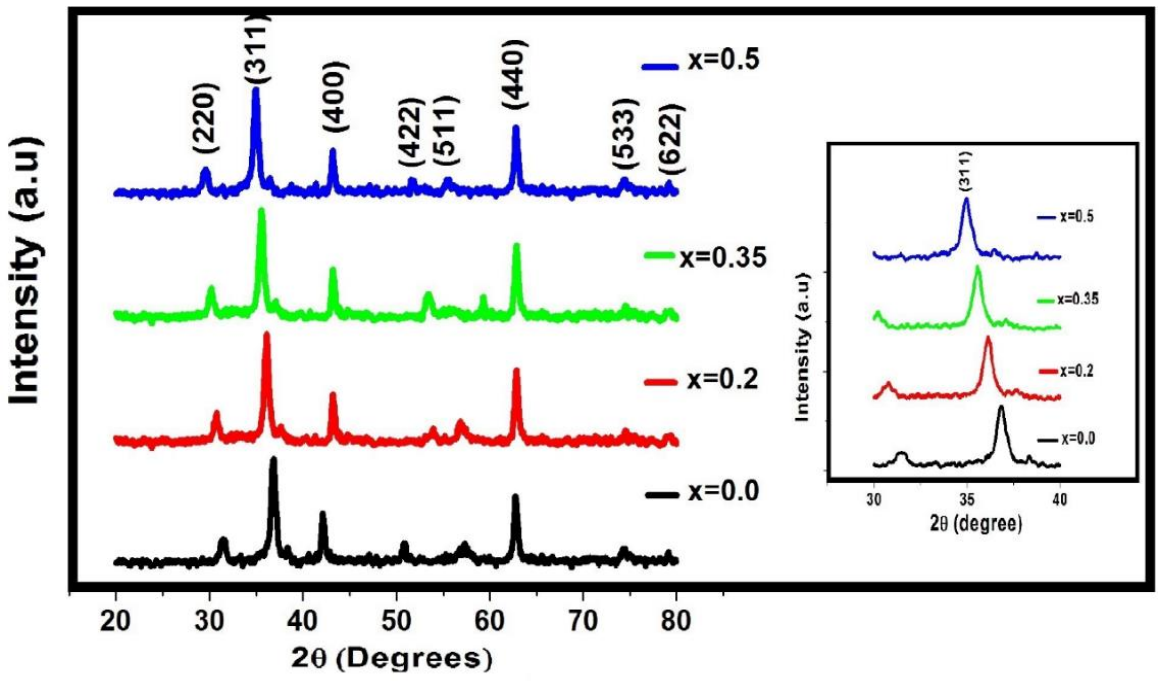

Figure 4.1: Indexed XRD pattern of $Mg_{1-x}Zn_xFe_2O_4$; x=0.0, x=0.2, x=0.35 and x=0.5

The diffraction patterns confirms the structure of the synthesized ferrites to be face centered cubic (FCC). The diffraction pattern is observed when condition of constructive interference for Bragg's Law is satisfied.

$n\lambda = 2d\sin\theta$

The structural analysis involving calculation of lattice parameter (a), crystallite size (D) mass density(ρm), XRD density (ρX) and porosity (P) of the annealed samples .No peaks of impurities were found in the diffraction pattern. Lattice constant can be measured by using the Bragg's law. For cubic structure the relation between lattice constant and the planar spacing is given by the following equation:

$$a = d_{hkl}\sqrt{h^2 + k^2 + l^2}$$

where d is the planar spacing and h, k and l are the Miller indices and lattice parameters (Fig 4.2) were found to be 8.08, 8.23, 8.36 and 8.49 A^o for all compositions.

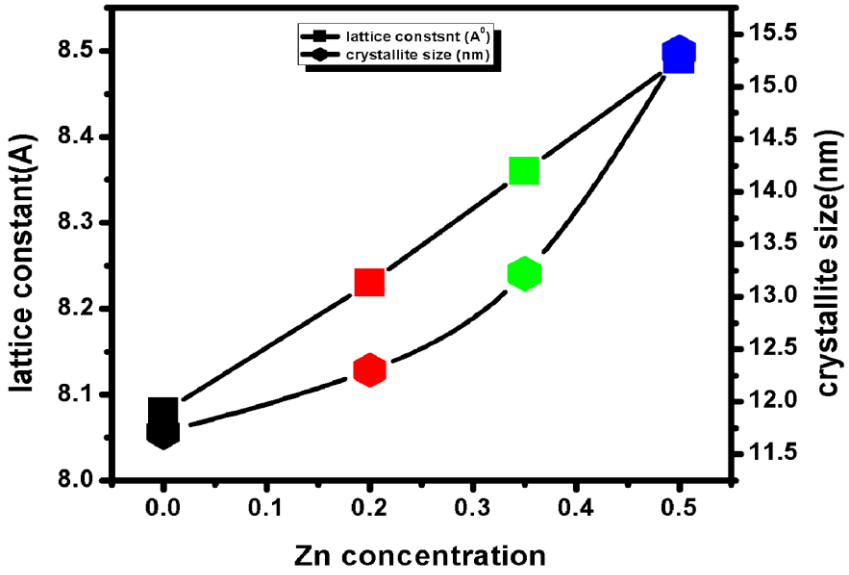

Figure 4.2: Lattice constants and crystallite size versus various compositions of Zn doped Mg ferrites.

Scherer formula [72] is used to calculate the average crystallite size.

The average value of crystallite size calculated is ~ 13.4 nm (Fig 4.2). From Fig 4.3 we get the decreasing trends of mass (ρ_m) and x-ray densities (ρ_{xrd}). Therefore the general decrease in porosity is predictable as shown in Fig 4.4.

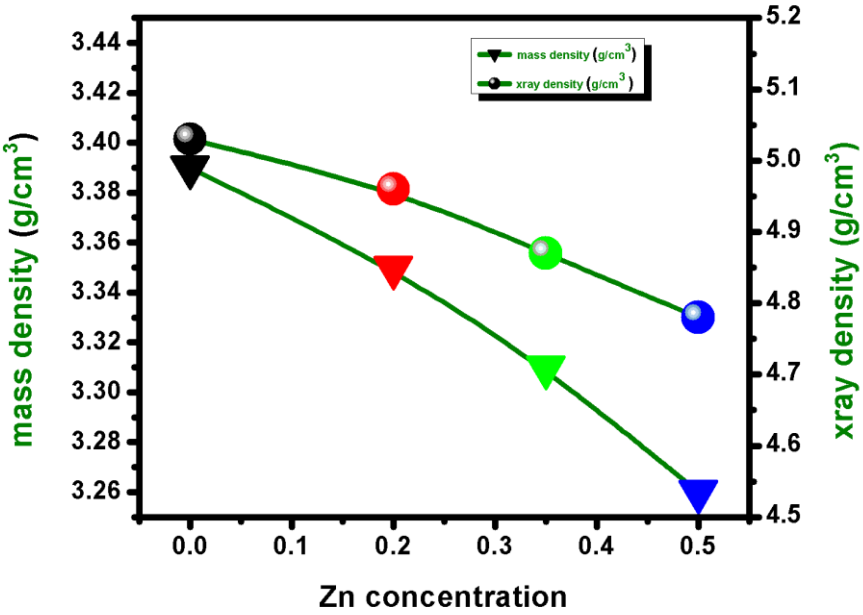

Figure 4.3: Variations of mass and x-ray densities of the samples.

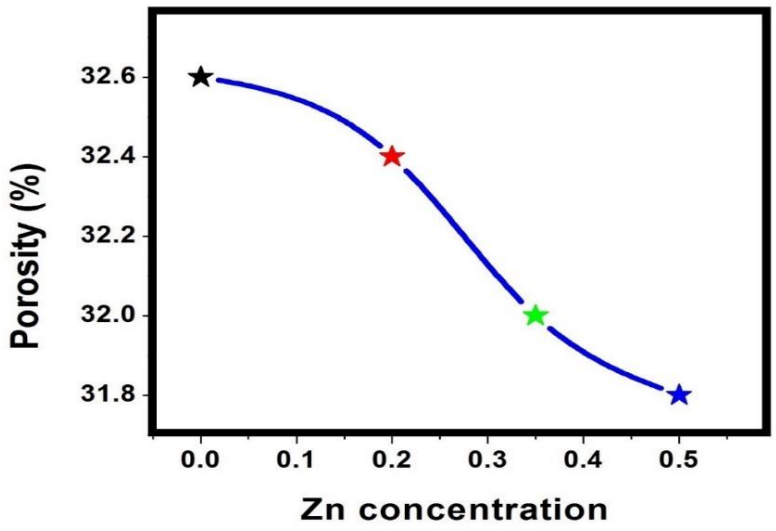

Figure 4.4: Porosity as a function of Zn doped content.

The whole structural status acquired is shown in Table 4.1, which are in agreement with the reported results [73]

Samples	$MgFe_2O_4$	$Mg_{0.8}Zn_{0.2}Fe_2O_4$	$Mg_{0.65}Zn_{0.35}Fe_2O_4$	$Mg_{0.5}Zn_{0.5}Fe_2O_4$
a (A^o)	**8.08**	**8.23**	**8.36**	**8.49**
V_{cell} (a^3)	**527.51**	**557.44**	**584.27**	**611.96**
D (nm)	**11.71**	**12.30**	**13.22**	**15.33**
ρ_m (g/cm^3)	**3.39**	**3.35**	**3.31**	**3.26**
ρ_x (g/cm^3)	**5.03**	**4.96**	**4.87**	**4.78**
P (%)	**32.6**	**32.4**	**32**	**31.8**

Table 4.1: Structural parameters: lattice constant (a), volume of the cell (V_{cell}), average crystallite size (D) for most intense crystalline peak (311), mass density (ρm), x-ray density (ρx) and porosity (P%) of $Mg_{1-x}Zn_xFe_2O_4$; x=0.0, x=0.2, x=0.35, x=0.5 samples.

4.2: Fourier transform infrared spectroscopy

The formation of spinel pure Mg Fe_2O_4 and Zn doped $MgFe_2O_4$ was further supported by FT-IR spectra (Fig 4.5) at room temperature. For the given samples, the structure of the spinel ferrites shows two absorption bands υ_1 and υ_2 , due to vibration of octahedral and tetrahedral metal oxygen bonds. Here, we have considered range of the absorption bands from 1000–300 cm^{-1} as suggested by previously published studies. In this range, a typical metal–oxygen absorption band for the spinel structure of the ferrite at ~ 414 and ~570 cm-1 was observed in the FT-IR spectra of all of the $Mg_{1-x}Zn_xFe_2O_4$ samples.

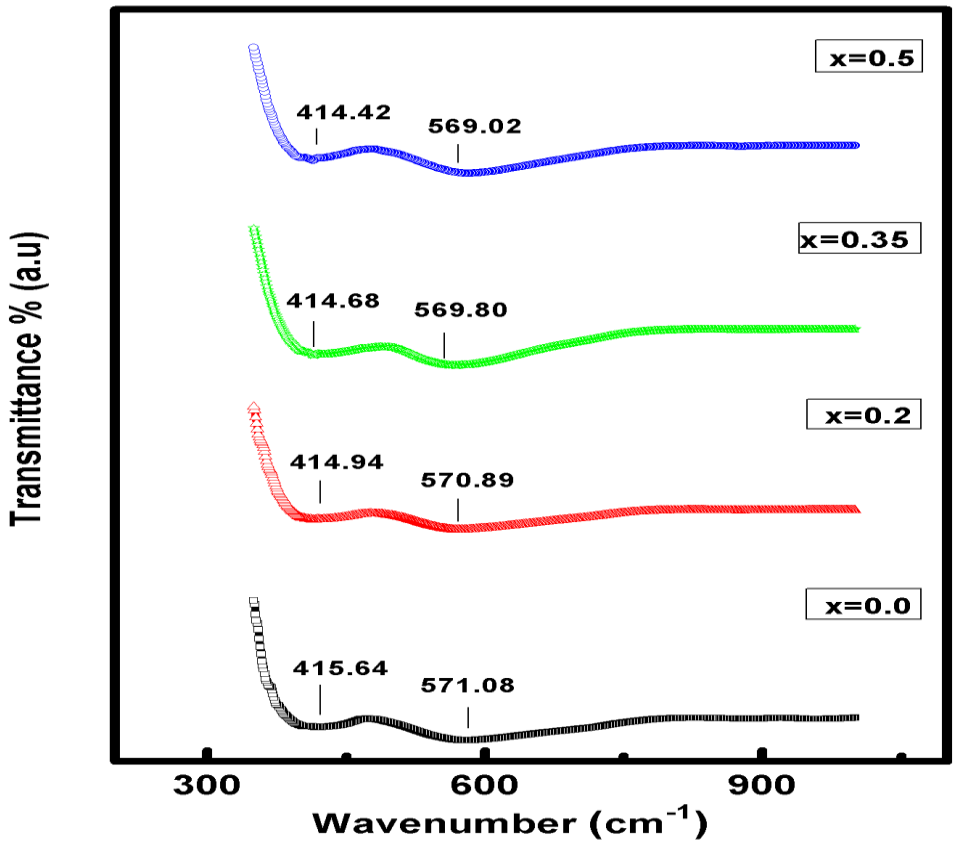

Figure 4.5: FTIR spectroscopy of $Mg_{1-x}Zn_xFe_2O_4$ samples

The intensity of the absorption bands depends generally on process of synthesis and substituted cation. The band υ_1 is for the tetrahedral position and υ_2 is for the octahedral position are stated in Table 4.2. The difference in the position of these two bands is due to the difference in bond length between metal and oxygen atoms at tetrahedral and octahedral sites. The absorption bands for the ferrites are found to be in the expected range. The high frequency band lie in the range 500–600 cm^{-1} while the low frequency band is lie in the 390–450 cm^{-1} range. The absorption peak centered at ~ 570 cm^{-1}, shifts to low wavenumber by increase in Zn content and can be related to the increase in distance between Fe^{3+}–O^{2-} in the tetrahedral sites.

Samples	*x=0.0*	*x=0.2*	*x=0.35*	*x=0.5*
υ_1	**571.08**	**570.89**	**569.80**	**569.02**
υ_2	**415.64**	**414.94**	**414.68**	**414.42**

Table 4.2: Tetrahedral and Octahedral band positions (υ_1, υ_2) of $Mg_{1-x}Zn_xFe_2O_4$ nanoparticles

5.3: SEM OF Zn substituted MgFe2O4 nanoparticles

To take the SEM micrographs of $Mg_{1-x}Zn_xFe_2O_4$ nanoparticles, a suspension was made in deionized water and sonicated for an hour. A small drop was then spread on a glass substrate which then heated to evaporate. After that, a thin layer of gold particles was coated on the above prepared sample to make it conductive for the machine. The microstructure of the sintered samples can be visualized from scanning electron microscope (SEM) tool. Fig 4.6 contains two SEM images with different concentration of Zn in Mg Ferrite.

These figures reveals that all the samples exhibit compact arrangement of homogeneous nanoparticles with spherical shape and porous structure which provides a larger specific surface area for the adsorption of gas. It was observed that the particle size increased from 16 to 20nm and consequently the porosity decreased, resulted in a homogeneous grain size distribution with increasing doping concentration. Some agglomeration can also be due to the Van Der Waals attraction and Brownian motion [74]

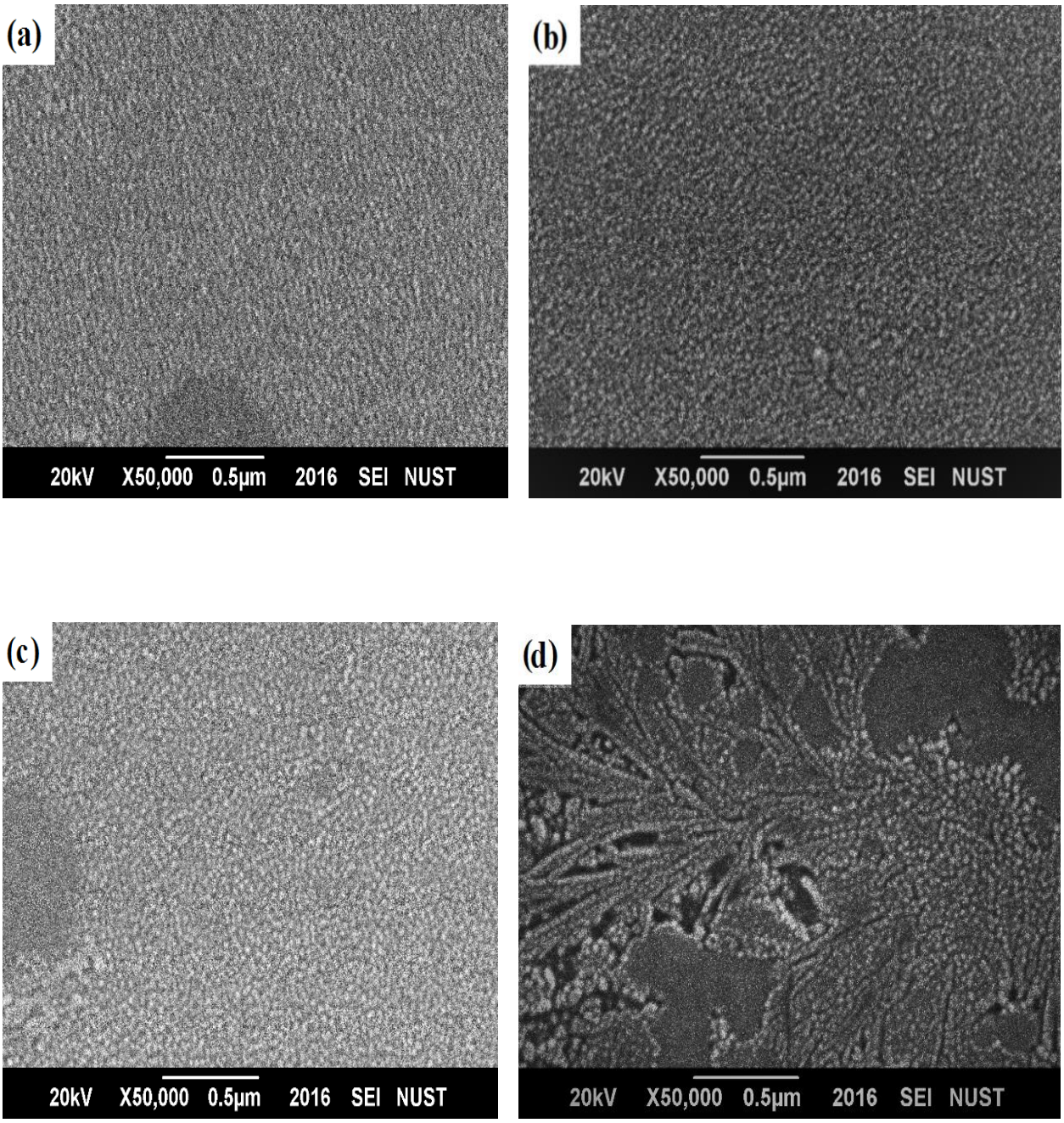

Fig 4.6: High resolution Sem micrographs of (a) $MgFe_2O_4$ (b) $Mg_{0.8}Zn_{0.2}Fe_2O_4$ (c) $Mg_{0.65}Zn_{0.35}Fe_2O_4$ (d) $Mg_{0.5}Zn_{0.5}Fe_2O_4$

4.4 UV-Vis spectral analysis

UV-vis spectral analysis has been widely used to characterize semiconductor nanoparticles. The absorption spectra of Mg ferrite and Zn doped in Mg ferrite nanoparticles ($Mg_{1-x}Zn_xFe_2O_4$) in UV-light region was illustrated in Fig 4.7. It can be clearly seen that all samples possessed an absorption band in the whole range as well as exhibited a good absorption in the light region (330-400 nm). The absorption at 330 nm is assigned to the characteristic absorption band of MgFe2O4 nanoparticles.

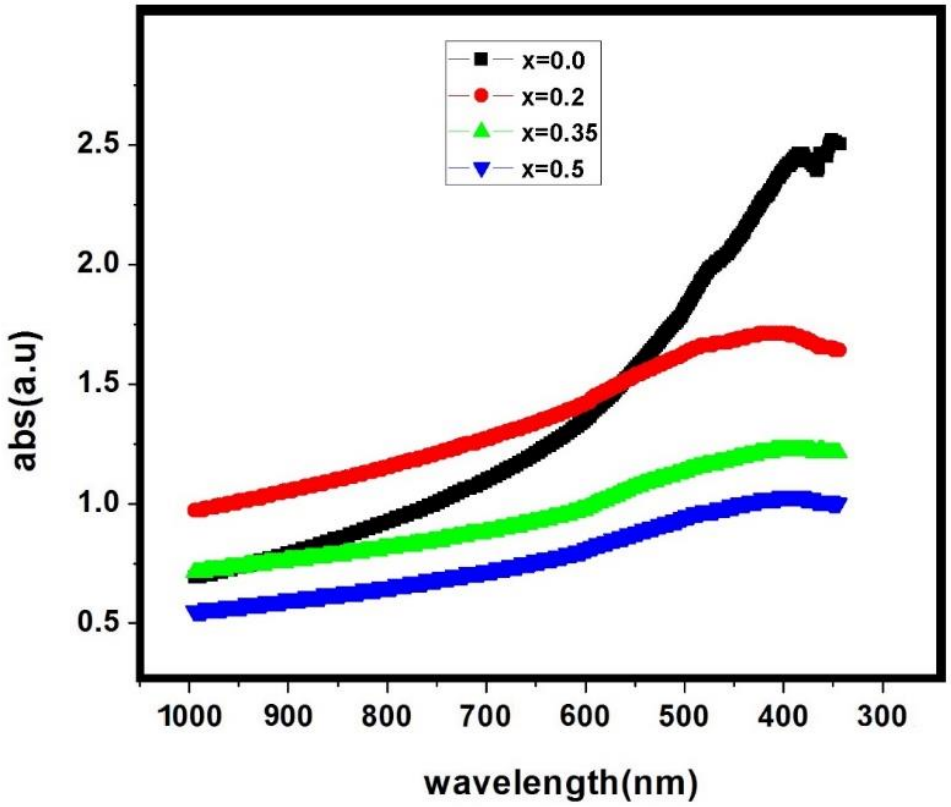

Figure 4.7: UV-Visible spectra of $Mg_{1-x}Zn_xFe_2O_4$; x=0.0, x=0.2, x=0.35, x=0.5

Determination of Band gap:

The fundamental absorption, which corresponds to electron excitation from the valance band to conduction band, can be used to determine the value of the optical band gap of the synthesized ferrite nanoparticles. The variation in the absorption coefficient (α) as a function of photon energy (hν) for allowed direct transitions (n=1/2) is given by:

$$\alpha h\upsilon = A(h\upsilon - Eg)^n$$

Where hυ is the photon energy, A is a constant, α is linear absorption coefficient. The Eg values are determined by extrapolating the linear portion of the Tauc plots between $(\alpha h\upsilon)^2$ versus hυ as shown in Fig 4.8 (a-d). Shows that the energy gap decreases with increasing doping content in Mg ferrite samples in the range 2.49 to 2.16 eV.

(a)

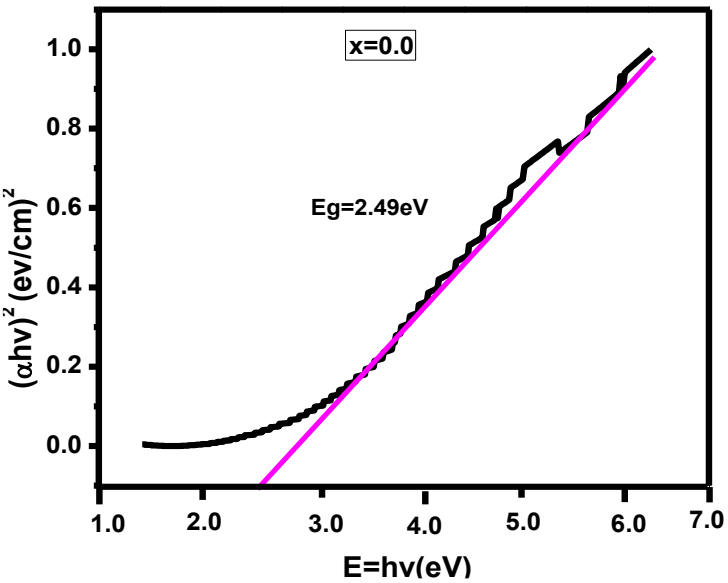

(b)

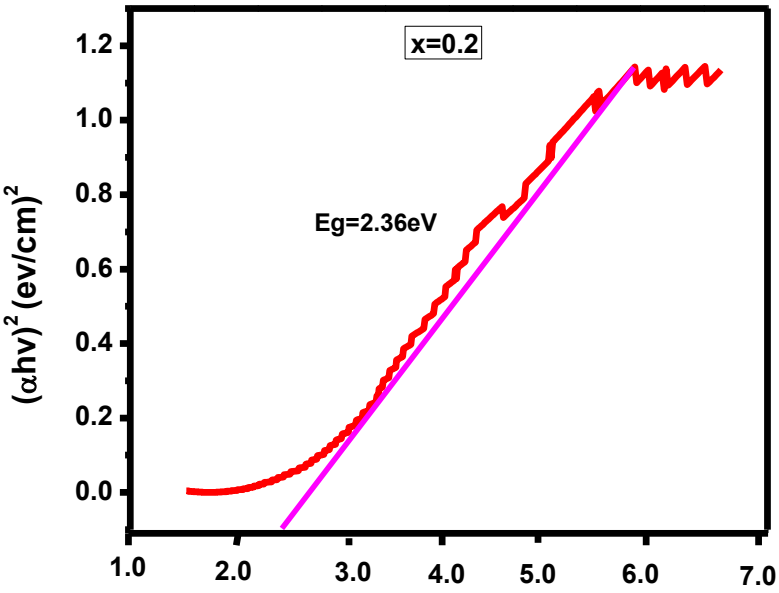
x=0.2
Eg=2.36eV
(αhv)² (ev/cm)²
1.2
1.0
0.8
0.6
0.4
0.2
0.0
1.0
2.0
3.0
4.0
5.0
6.0
7.0

(c)

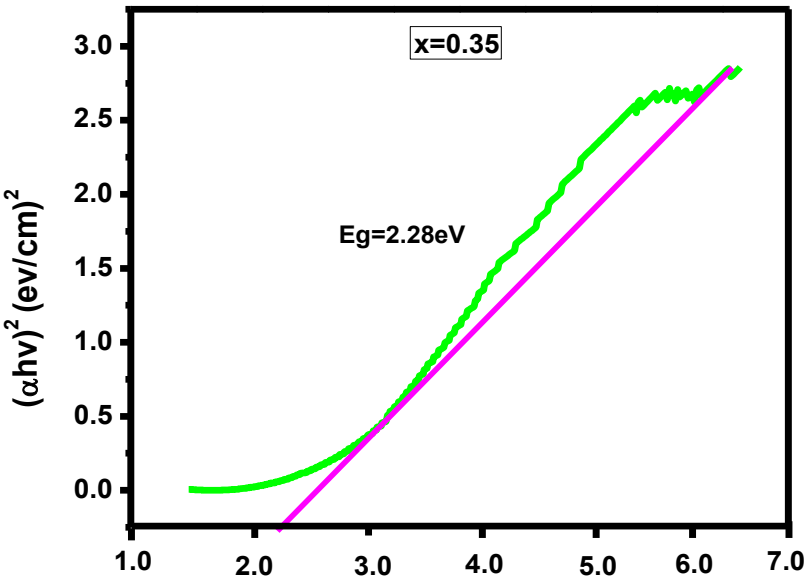
x=0.35
Eg=2.28eV
(αhv)² (ev/cm)²
3.0
2.5
2.0
1.5
1.0
0.5
0.0
1.0
2.0
3.0
4.0
5.0
6.0
7.0

(d)

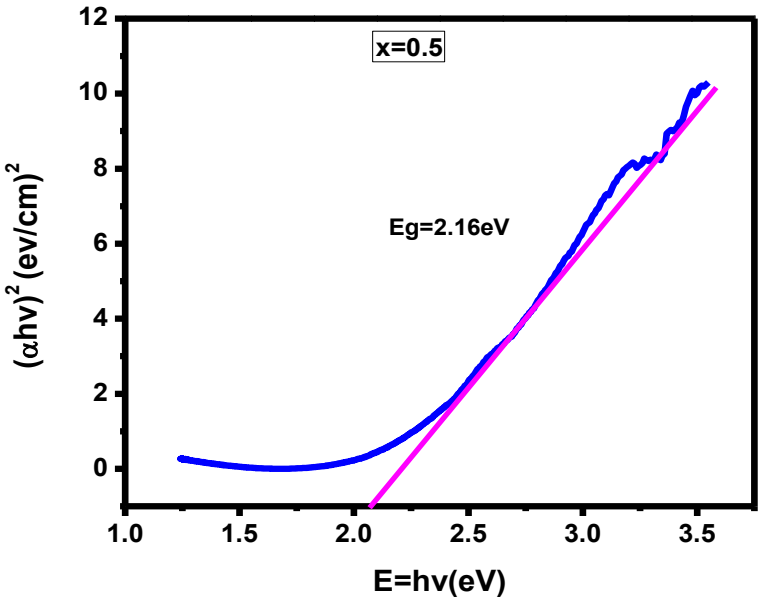

Figure 4.8: Tauc plots for Energy gap spectra of Mg-Zn ferrites

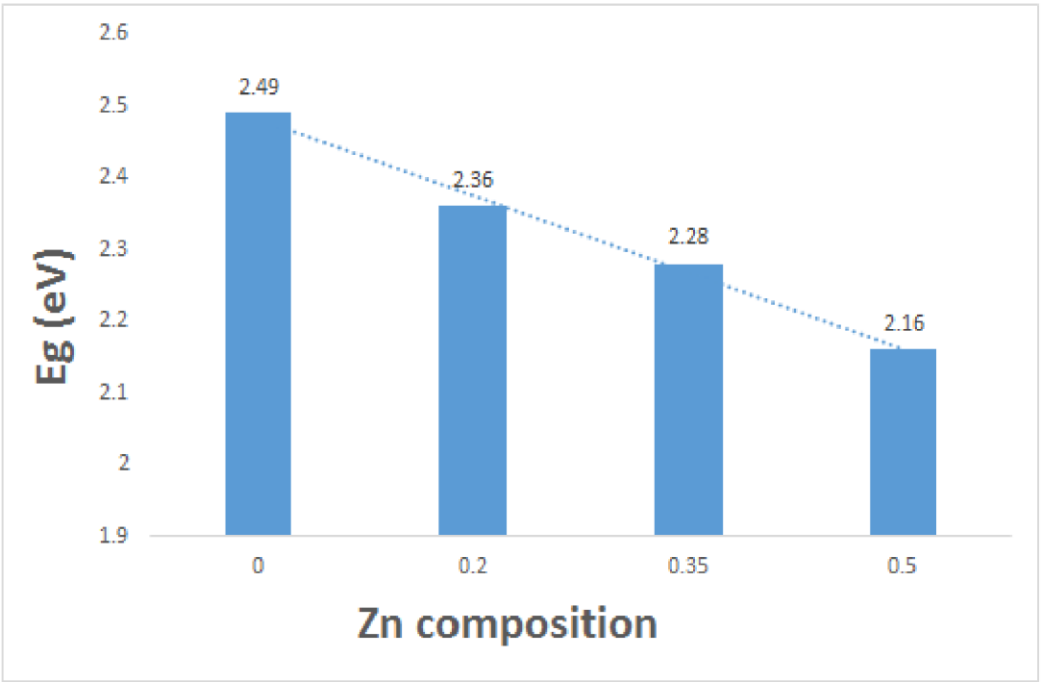

Figure 4.9: Variation of band gap with different compositions of Mg-Zn Ferrites.

4.5: Dielectric measurements

Figs 4.10 and 4.11 indicate the variation of dielectric constant and dielectric loss with frequency reveals the dispersion due to Maxwell–Wagner

type interfacial polarization in agreement with Koop's phenomenological theory [76]

The dielectric constant decreases with increasing frequency reaching a constant value for all the samples. According to Rabinkin and Novikova [77]

the polarization in ferrites is through a mechanism similar to the conduction process. By electron exchange between $Fe^{2+} \leftrightarrow Fe^{3+}$, one obtains local displacement of electrons in the direction of the applied field and these electrons determine the polarization. The large values of ε' at lower frequencies are due to the high proportion of the species like Fe^{2+} ions, oxygen vacancies, grain boundary defects, etc. While the decrease in ε' with frequency is natural because of the fact that any species contributing to polarizability is bound to show lagging behind the applied field at higher frequencies. Structural defects give rise to trapping centers for the electrons, also known as correlated states. It thus follows that loss factors at the higher frequency corresponds to the hopping of electrons. As at low frequency region where $\omega < 1/\tau$, hopping of ions plays an important role, ω is the angular frequency and τ is relaxation time).

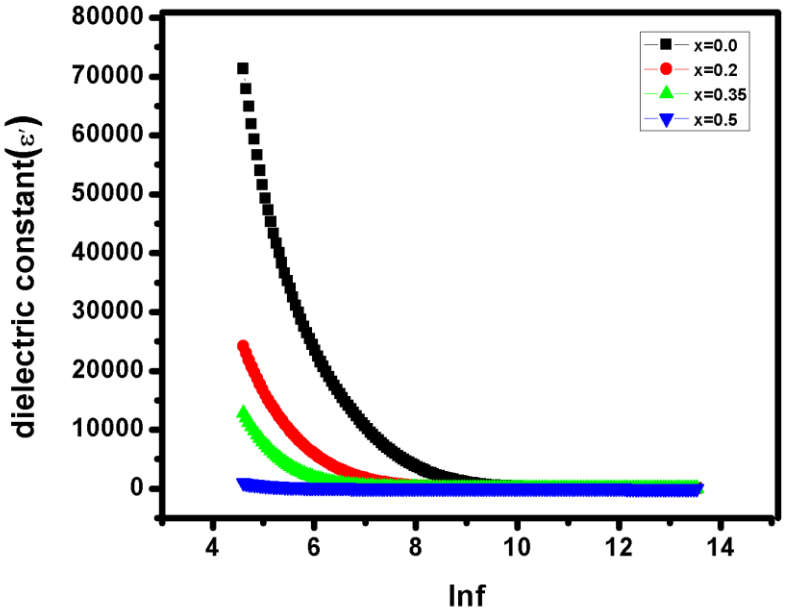

Figure 4.10: Dielectric constant as a function of frequency for $Mg_{1-x}Zn_xFe_2O_4$ samples.

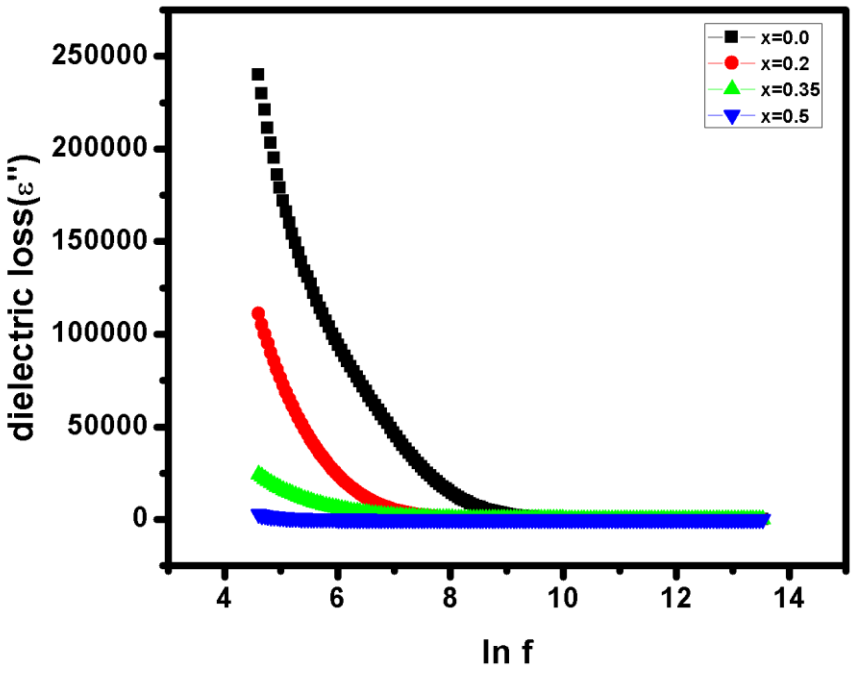

Figure 4.11: Dielectric loss plots for $Mg_{1-x}Zn_xFe_2O_4$ samples.

At higher frequencies hopping of ions ends due to prompt fluctuation of the applied field and random orientations of dipolar moments which tends to decrease the value of ε′. After specific range of frequency dielectric constant becomes constant for higher range frequencies. This shows dependency of both dielectric constant and dielectric loss factor on frequency [78

The applied electric field created the dipole moments which are well aligned due to hopping mechanism. Figure 8b represents the dielectric loss factor versus frequency for $Mg_{1-x}Zn_xFe_2O_4$ samples for different compositions. At higher frequency, a relaxation phenomenon of electric field in materials take place. Decrease of dielectric loss factor at higher frequency region also credited towards the purity of prepared materials and corresponds to the good optical properties which in return could be useful in industry for designing many optical devices [79]].

.

The variation of tangent loss (tan δ) with frequency is shown in Fig 4.12. All the samples show dispersion in tan δ as in agreement with Maxwell-Wagner Model which also validates Koops theory. A maximum value of tan δ is observed when the hopping frequency of electron between Fe^{2+} and Fe^{3+} is equal to the frequency of the applied field. The conduction mechanism in n-type ferrites is considered as due to hopping of electrons between Fe^{2+} and Fe^{3+} situated on the octahedral sites [80] As such when the hopping frequency is nearly equal to that of externally applied field a maximum of loss tangent may be observed. Tangent loss actually reveals the amount of dissipated energy in the material in the presence of external applied field. Actually there is shift in the phase at specific frequency where loss of energy takes place. Generally losses occurs when polarization of dipoles is unfollowed by the electric field. Consequently at higher frequencies tangent loss decreases and at 14 MHz, tan δ is almost zero. This property enables these materials to capable for designing high frequency devices. Almost same trend is observed for all synthesized samples [81]

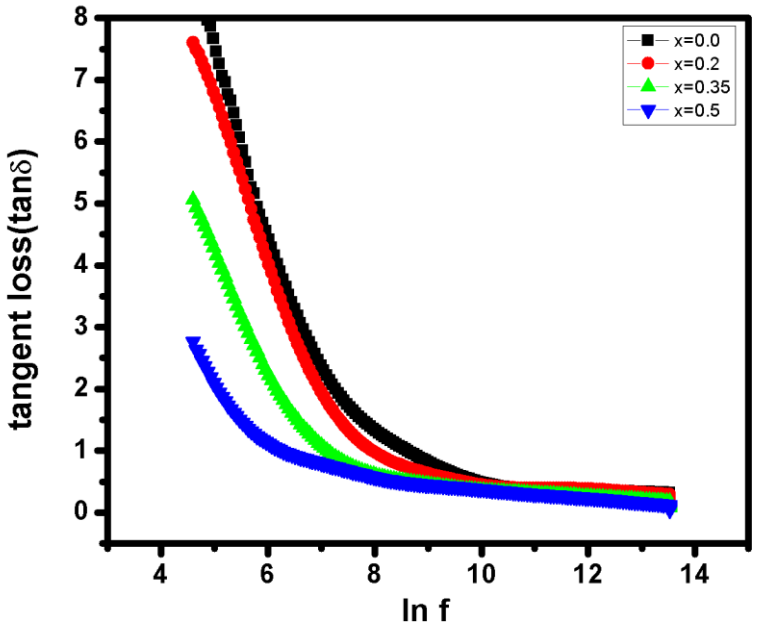

Figure 4.12: Tan loss curves for $Mg_{1-x}Zn_xFe_2O_4$ samples

.

By measuring tangent loss factor, dielectric constant and frequency, ac conductivity can be easily measured. It can be seen from the curves in Fig. 4.13 that at lower frequency AC conductivity is low but with increase in frequency AC conductivity also increases. This type of behavior confirms the semiconductor nature of ferrite nanoparticles. The AC trend observe in Mg-Zn ferrites nanostructures is mainly due to relaxation and hopping mechanism. The ac conductivity is measured as a function of frequency at room temperature. In semiconductor materials the hopping takes place between the localized states lies within the band gap. At room temperature the mechanism of exciton hopping occurs repeatedly and leading to large hopping distance [82]

.

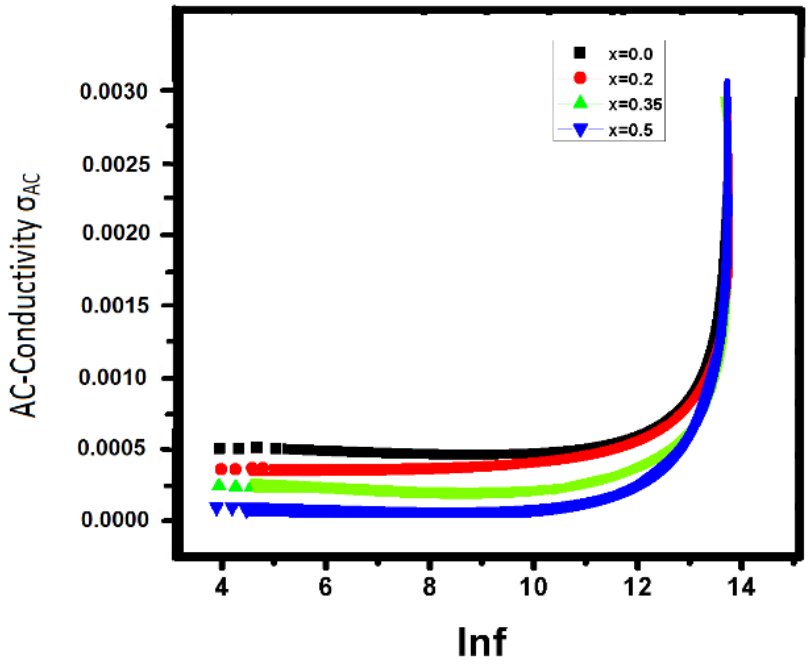

Figure 4.13. AC conductivity of $Mg_{1-x}Zn_xFe_2O_4$ samples ranging from x=0.0-0.5

4.6 Gas sensing properties of Zn doped MgFe2O4

Gas sensing properties plays an important role for various necessities including detection of explosive gases, environmental protection, and to detect combustible gases. The gas sensing

property of different gases is based on the adsorption and desorption process. The amount of absorbed oxygen species is quite important for providing enough reactants for the reactions.

It can be seen from Fig 4.14 that the resistance increased in the presence of air with time and at the insertion of CO_2 it start decreasing for Zn doped $MgFe_2O_4$ samples, showing the dependence of resistance of sensor elements on response time. All prepared samples has shown a very precise response time of 1 min for the detection of CO_2 gas.

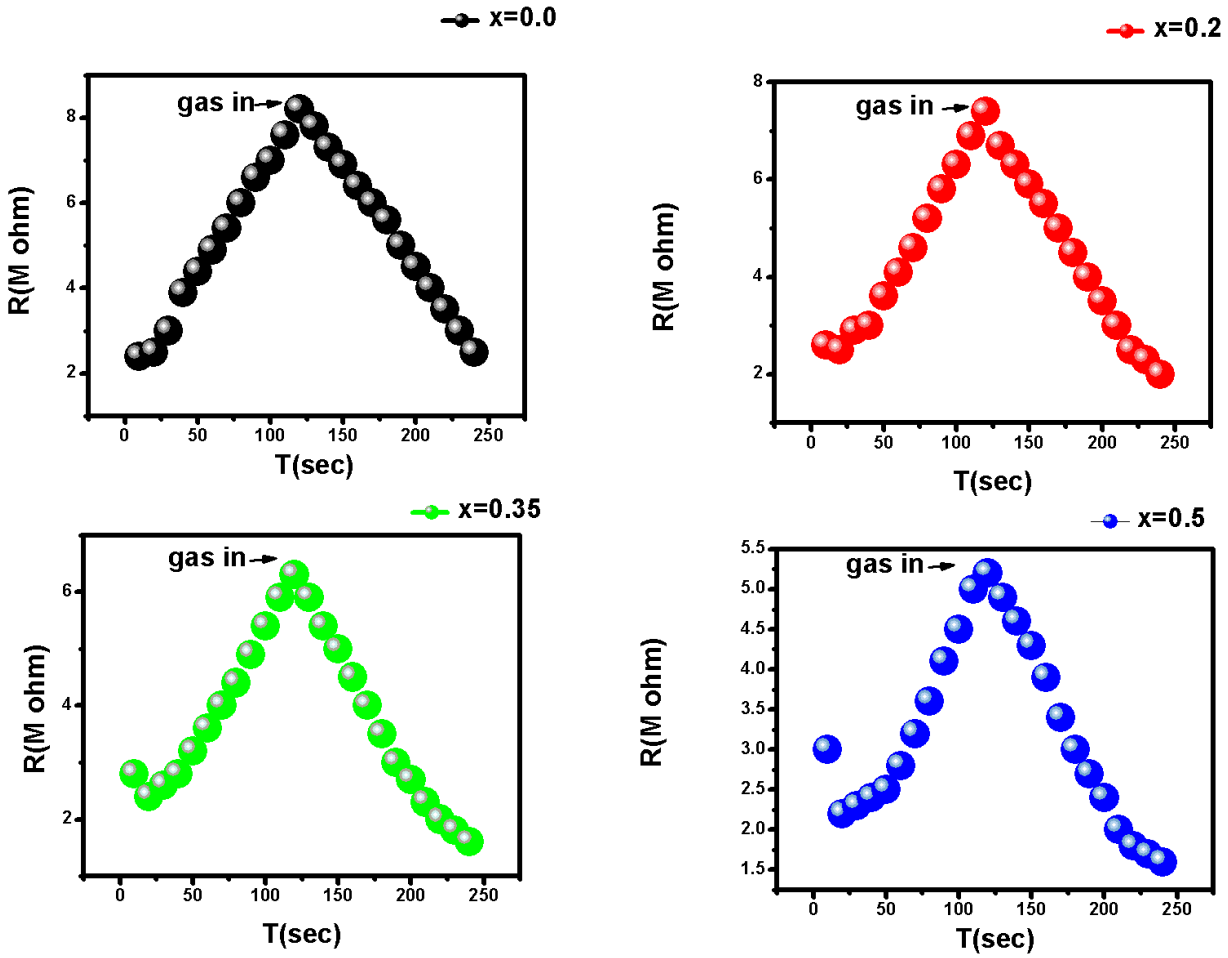

Fig 4.14: Resistance transient of $Mg_{1-x}Zn_xFe_2O_4$ for CO_2

From Fig 4.15 (a-d), we note that the sensor resistance increases at an initial stage but decreases afterwards with the time at the exposure of gas. This can be explained qualitatively from a dynamic balance between initial fast adsorption of exposed gas molecules and the further acceleration of desorption. Moreover, this can also be understood by considering the reaction rate between the gas

and the sensing material increases as time increases and further decrease due to the combustion of the tested gas.

(a)

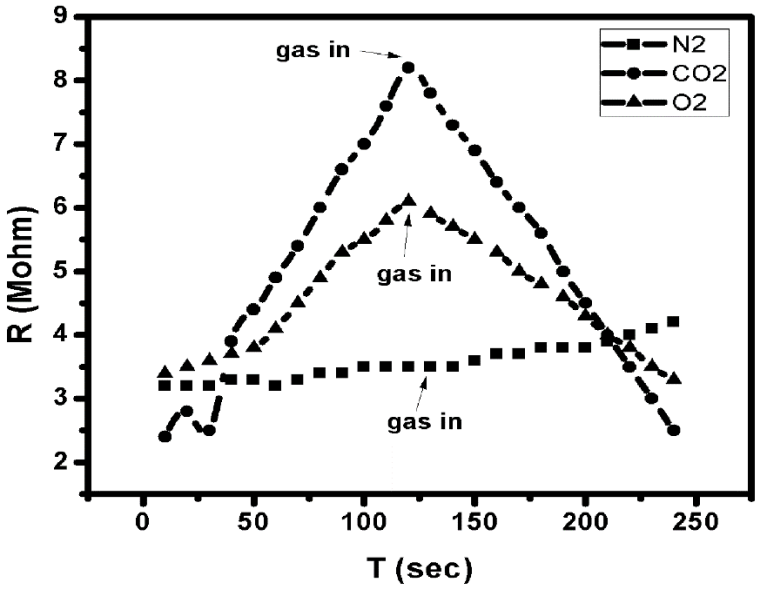

(b)

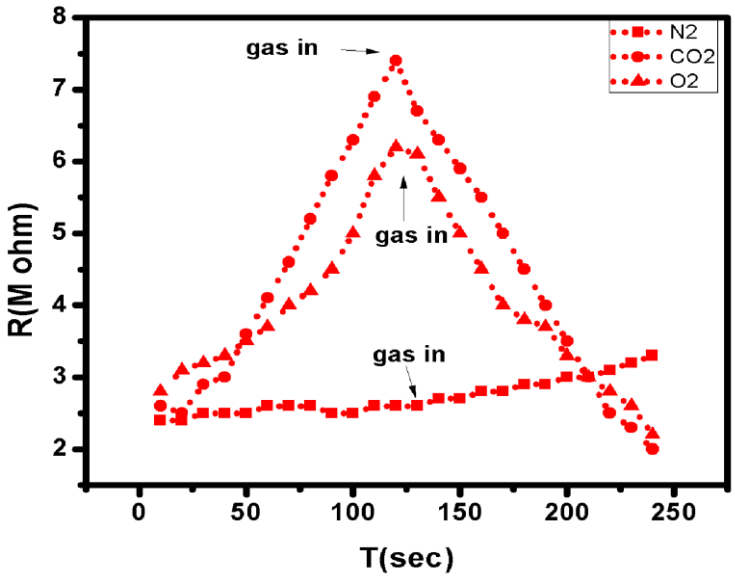

(c)

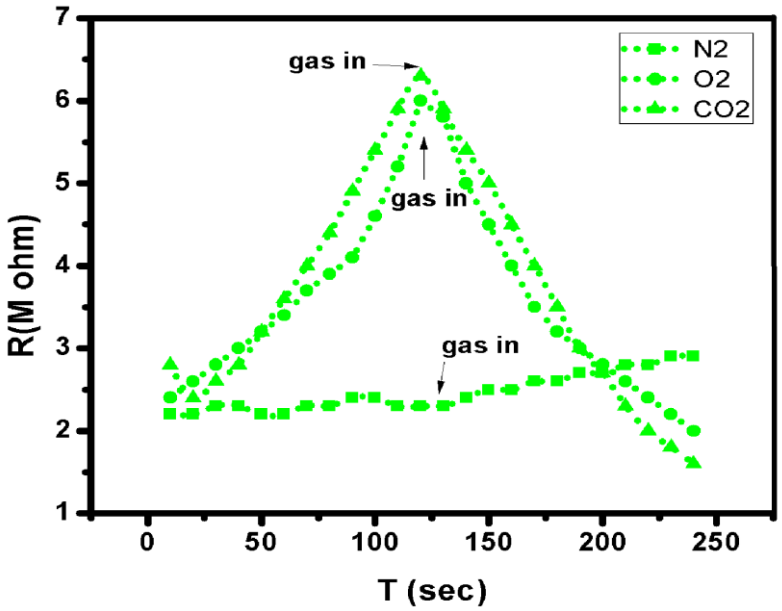

(d)

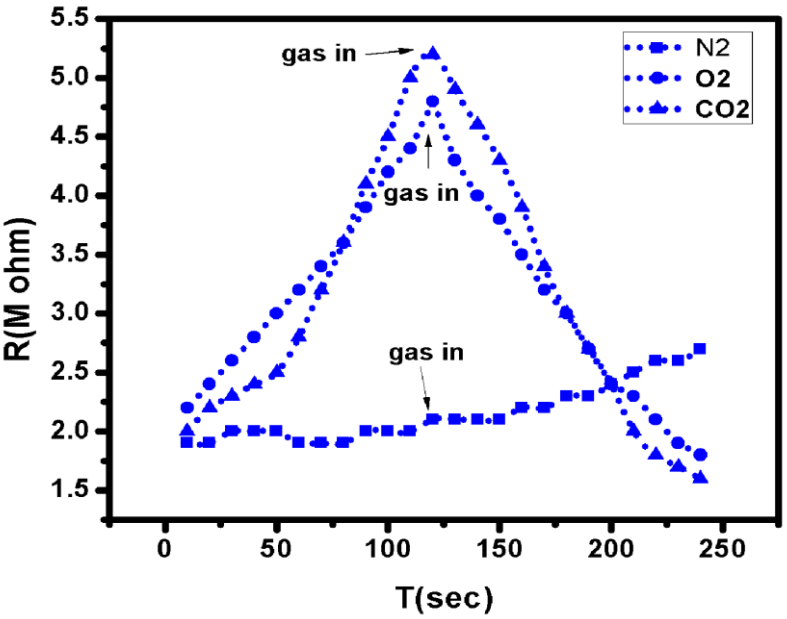

Figure 4.15: The resistance transient of $Mg_{1-x}Zn_xFe_2O_4$ (a) x=0.0 (b) x=0.2 (c) x=0.35 (d) x=0.5 samples for CO_2, O_2 and N_2.

The sensitivities of the four ferrites towards the gases, CO_2, O_2 and N_2 are compared in Fig 4.16 as a function of composition, showing decrease in sensitivities due to decrease in number of pores with increasing doping content. The Nano structured samples showed maximum sensitivity (Eq. 1) to CO_2 gas at room temperature, whereas sensitivity to other gases was comparatively low as depicted in Fig. 4.17, showed exclusive selectivity to CO_2 for the Zn doped Mg ferrites-based sensors. The sensing characteristics give an idea of the response time and defined as the time taken by the sensor to reach 75% of the final response. It is found that $Mg_{1-x}Zn_xFe_2O_4$ shows a rise time (response time) of ~ 60–70 s for CO_2. Detailed gas sensing parameters are shown in Table 2.

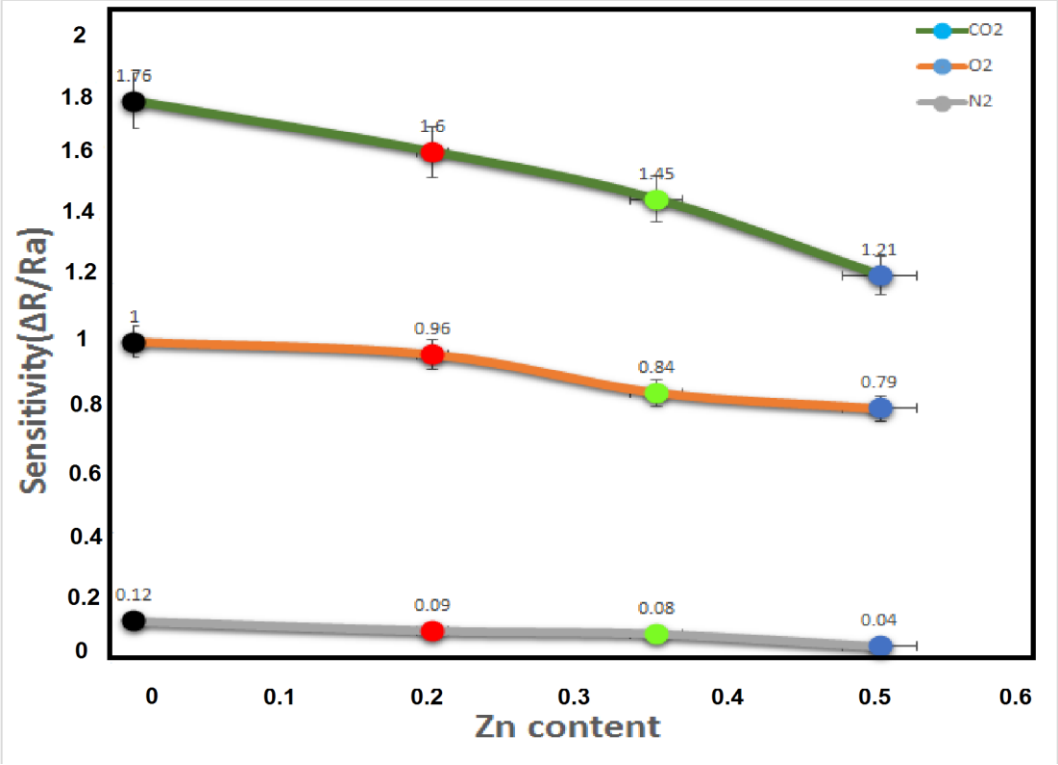

Figure 4.16. Sensitivity as a function of Zn doped Mg ferrites.

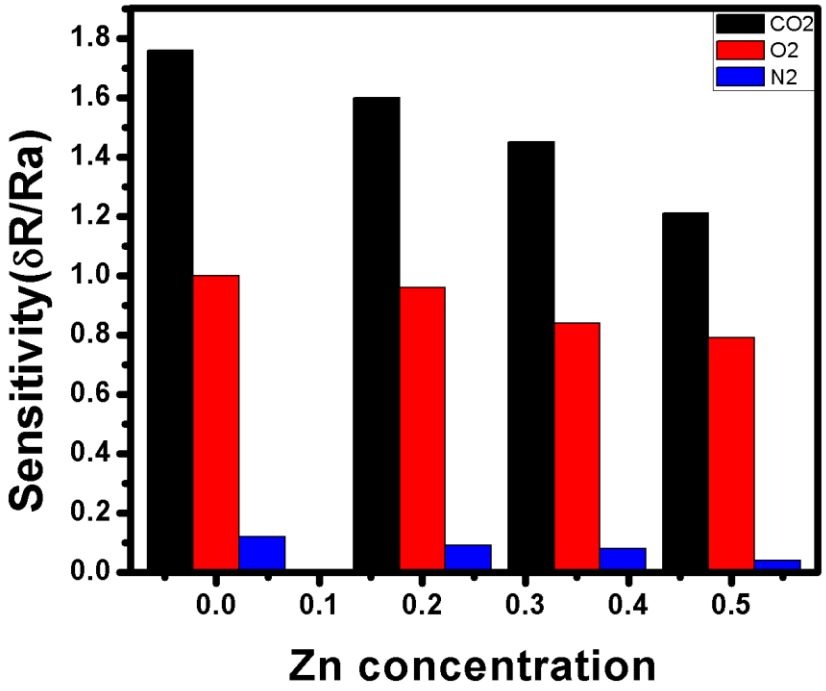

Figure 4.17: Change in sensitivity vs composition among various gases.

Samples	*CO2*		*O2*		*N2*	
	Sensitivity S=|ΔR|/Ra	*Response Time (sec)*	*Sensitivity S=|ΔR|/Ra*	*Response Time (sec)*	*Sensitivity S=|ΔR|/Ra*	*Response Time (sec)*
$MgFe_2O_4$	1.76	~65	1	~75	0.12	~120
$Mg_{0.8}Zn_{0.2}Fe_2O_4$	1.60	~66	0.96	~77	0.09	~122
$Mg_{0.65}Zn_{0.35}Fe_2O_4$	1.48	~69	0.87	~79	0.08	~126
$Mg_{0.5}Zn_{0.5}Fe_2O_4$	1.21	~70	0.79	~80	0.04	~130

Table 4.3: Gas sensing characteristics (sensitivity, response time) of $Mg_{1-x}Zn_xFe_2O_4$; x=0.0, x=0.2, x=0.35, x=0.5

CHAPTER 5

SUMMARY, CONCLUSION & FUTURE RECOMMENDATION

The materials that were investigated during the course of this thesis are spinel type ferrites and considered to be the most promising materials for study of sensors because of their high surface to volume ratio. Spinel type ferrites are very versatile gas sensing materials that with continued development will show greater industrial applications. This research attempts to explain the synthesis techniques their characterization methods, and gas sensing requirement of Mg-Zn ferrite nanomaterials.

Mg_{1-x} $Zn_xFe_2O_4$ (x=0.0, 0.2, 0.35, 0.5) samples were prepared by the co-precipitation method and well characterized by X-ray diffraction and SEM, through which samples were found to be cubic spinel ferrite nanoparticle structure, having lattice parameter 8.08, 8.23, 8.36 and 8.49 A^o and grain size in the range of 11-16nm. Differences in crystallinity, surface area, particle size and optical properties of the ferrite NPs with different concentration of Zn doping were observed. It is observed that both the crystallite size and the lattice parameter of nano ferrites are found to increase with increasing doping content. The structural formation of ferrites was then confirmed by FTIR spectra, showing band ranges of 500–600 cm^{-1} for tetrahedral and 390–450 cm^{-1} for octahedral lattice sites. The absorption bands are found in the expected range and the difference in band positions is due to the difference in the Fe^{3+} - O^{2-} for the octahedral and tetrahedral complexes. The positions absorption bands are compositional dependent whose dependence could be attributed to the variation in cation oxygen bond distances. UV– Vis absorption spectroscopy shows that the energy band gap of the synthesized Mg_{1-x} $Zn_xFe_2O_4$ nanoparticles decreases by increasing doping contents, in the range from 2.49 to 2.16 eV. Dielectric study showed a very low dielectric loss of Zn doped magnesium ferrites at frequencies over 10 MHz. It follows that samples with the composition x=0.5 has not only a uniformly low dielectric constant at all frequencies, it also shows a low loss factor. These are the desirable features in most of the devices, such devices can be successfully operated over a wide frequency range.

$Mg_{1-x}Zn_xFe_2O_4$ nanoparticles showed greater sensitivity to CO_2 as compared to O_2 and N_2. The sensor showed good response (~ 1min) to CO_2 gas. It was observed that the gas sensitivity depends on types of semiconducting material, concentration of dopants and test gases to be detected and

concluded that ferrite materials have useful properties and applications in the field of sensors at room temperature.

In the future it would be interesting to work on the following aspects

- This developing research will lead the future industry, for the development of high-quality ferrites i.e. Mg ferrite as gas sensors for industrial processes and other applications.
- Moreover, due to temperature dependent sensing response and sensitivity, the same sensor can be used for detection of variety of gases at higher temperatures.
- Further studies can be carried for improving the sensor's performance characteristics with respect to sensitivity, response time, doping content and temperature.

Reference:

[1] http://www.zyvex.com/nanotech/feynman.html

[2] http://www.kheper.net/topics/nanotech/nanotech-history.htm

[3] Drexler, K. Eric. "Introduction to nanotechnology." Proceedings of the first general conference on Nanotechnology: development, applications, and opportunities: development, applications, and opportunities. John Wiley & Sons, Inc., 1995

[4] www.foresight.org › About Nanotechnology

[5] futurehumanevolution.com/history-of-nanotechnology-updated

[6] http://biologicalfuelcell.wordpress.com/biological-fuel-cells

[7] J.S. Kim, A.E. Kuk, B.K.N. Yu, Nanomed. Nanotechnol. Biol. Med. 3, 95, 2007

[8] J. Shi, Y.Zhu, X. Zhang, Willy R.G. Baeyens, Ana M. GarcaiaCampana, Trends in Analytical Chemistry, 23, 351, 2004

[9] P. Liu, M. Zhao, Appl. Surf. Sci. 255, 3989, 2009

[10] https://www.wiley-vch.de/books/sample/3527407901_c01.pdf

[11] www.winnerscience.com/nanotechnology-2/surface-area-to-volume-ratio-in nanoparticles

[12] www.nobraintoosmall.co.nz/students/biology/NCEA.../bio2_91156_satovolume.pdf

[13] http://www.nanowerk.com/nanotechnology/introduction/introduction_to_nanotechnology_3.php

[14] copublications.greenfacts.org › Home › Nanotechnologies › Level 2

[15] https://en.wikipedia.org/wiki/Nanoparticle

[16] www.dummies.com/how-to/content/how-materials-change-in-nanoscale.html

[17] http://www.pharmainfo.net/book/emerging-trends-nanotechnology-pharmacy-1introduction-nanotechnology/physical-and-chemical

[18] Guo, Dan, Guoxin Xie, and Jianbin Luo. "Mechanical properties of nanoparticles: basics and applications." Journal of Physics D: Applied Physics 47.1 (2013): 013001

[19] Lubick N, Betts K (2008).Silver socks have cloudy lining". Environ Sci Technol 42 (11): 3910. Bibcode:2008EnST.42.3910L

[20] Vollath D. Nanomaterials: An Introduction to Synthesis,Properties and Application. November/December 2008, Vol. 7, No.6, 865-870.http://omicron.ch.tuiasi.ro/EEMJ

[21] www.sciencedaily.com/releases/2010/05/100531082857.htm

[22] http:\www.nanostrast.d/index-php/en/nanotechnology-information/610-Schneller-Sparamer-roboster-nanotechnologie-in-computer-handy-a-io

[23] ec.europe.eu/consumers/sectors/cosmetics/cosmeticproducts/nanomaterials/index en.htm

[24] Http://en.wikipedia.org/wiki/carbonnanotube

[25] Callister, W. (2003). Materials science and engineering an introduction. Sixth ed. New York: JoHn Wiley & Sons, Inc

[26] Spaldin, N. (2003). Magnetic materials: Fundamentals and device aplications. Cambridge: Cambridge University press

[27] Goldman, A. (1990).Modern Ferrite Technology. Van Nostrand Reinhold, New York

[28] H.S.C. O'Neill, A. Navrotsky, Simple spinels: crystallographic parame-ters, cation radii, lattice energies, and cation distribution, Am. Mineral. 69(1983) 181–194.[19] H.B. Callen, S.E. Harrison, C.J. Kriessman, Cation distribution in ferro-spinels, Theor. Phys. Rev. 103 (1956) 851–856

[29] C.R. Vestal, J.Z. Zhang, Magnetic spinel ferrite nanoparticles frommicroemulsions, Int. J. Nanotechnol. 1 (2004) 240–263

[30] Bragg, W. H. (1915 a), Nature 95, 561

[31] Bragg, W. H. (1915 b), Phil. Mag. 30, 305

[32] Mehdiye, T.R., Gashimov, A.M., and Habibzade, A.A., (2008). Electromagnetic Processes in frequency-dependent resistor sheath.Fizika Cild Xiv №3 p 80-88

[33] Daliya S. M., and Juang, R. S. (2007). An overview of the structure and magnetism of spinel ferrite nanoparticles and their synthesis in micro emulsions. Chemical Engineering Journal, 129 (1-3): 51–65

[34] Jiles, D. (1991). Introduction to Magnetism and Magnetic Materials. (First ed) Londond: Chapman & Hall

[35] C.O. Park, S.A. Akbar "Ceramics for chemical sensing" J. Mater. Sci., 38 (2003), pp. 4611–4637

[36] X.J. Huang, Y.K. Choi "Chemical sensors based on nanostructured materials
Sens. Actuators" B-Chem., 122 (2007), pp. 659–671

[37] J. Kong, N.R. Franklin, C. Zhou, M.G. Chapline, S. Peng, K. Cho, H. Dai
"Nanotube molecular wires as chemical sensors Science", 287 (2000), pp. 622–625

[38] E. Llobet Gas sensors using carbon nanomaterials: a review, Sens. Actuators B-Chem., 179 (2013), pp. 32–45

[39] U. Lange, N.V. Roznyatovskaya, V.M. Mirsky "Conducting polymers in chemical sensors and arrays" Anal. Chim. Acta, 614 (2008), pp. 1–26

[40] H.J. Kim, J.H. Lee Highly sensitive and selective gas sensors using p-type oxide semiconductors: overview, Sens. Actuators B-Chem., 192 (2014), pp. 607–627

[41] G. Korotcenkov Metal oxides for solid-state gas sensors: what determines our choice?
Mater. Sci. Eng. B, 139 (2007), pp. 1–23

[42] I.S. Hwang, J.H. Lee, S.G. Oha, I.D. Kim, Microstructural control and selective C_2H_5OH sensing properties of Zn_2SnO_4 nanofibers prepared by electrospinning, Chem. Commun., 47 (2011), pp. 9315–9317

[43] N. Yamazoe, New approaches for improving semiconductor gas sensors, Sens. Actuators B-Chem., 5 (1991), pp. 7–19

[44] http://www.researchgate.net/ figure/281404855 fig3_Fig 3 Gas-sensing-mechanism-of-chemical-semiconductor-oxide-gas-sensors

[45] A. Sutka, G. Mezinskis, M. Zamovskis, D. Jakovlevs, I. Pavlovska, Monophasic ZnFe2O4 synthesis from a xerogel layer by auto combustion, Ceram. Int., 39 (2013), pp. 8499–8502

[46] Iqbal, Parvez, Jon A. Preece, and Paula M. Mendes. "Nanotechnology: The "Top-Down" and "Bottom-Up" Approaches." Supramolecular Chemistry: From Molecules to Nanomaterials (2012)

[47] http://www.pharmainfo.net/book/emerging-trends-nanotechnology-pharmacy-1introduction-nanotechnology/techniques-convert

[48] Pierson, H. (1999) Fundamentals of Chemical Vapor Deposition. In Handbook of Chemical Vapour Deposition (CVD) (2nd Ed.). Elsevier

[49] Wright, J., & Sommerdijk, N. (2000) Sol-Gel Materials Chemistry

[50] S. Ghosh, S. Dasgupta, A. Sen, and H. S. Maiti, ‘‘Low Temperature Synthesis of Bismuth Ferrite Nanoparticles by a Ferrioxalate Precursor Method,’’ Mater.Res. Bull., 40 [12] (2005). 2073

[51] T.-J. Park, G. C. Papaefthymiou, A. J. Viescas, A. R. Moodenbaugh, and S. S. Wong, ‘‘Size-Dependent Magnetic Properties of Single-Crystalline Multiferroic $BiFeO_3$ Nanoparticles,’’ Nano Lett. 7 [3] (2007) 766

[52] http://www.cresp.org/NuclearChemCourse/monographs/09_Jarvinen_FuelCycleSep%20

[53] https://www.mrl.ucsb.edu/centralfacilities/x-ray/basics

[54] W.D. Callister, D.G. Rethwisch, Materials Science and Engineering: An Introduction, John Wiley & Sons Canada, Limited, 2010

[55] Z. Guo, L. Tan, Fundamentals and Applications of Nanomaterials, Artech House, Incorporated, 2014

[56] http://science.howstuffworks.com/scanning-electron-microscope

[57] http://www.analyticalspectroscopy.net/ap3-8.htm

[58] W.D. Perkins (1986)"Fourier Transform-Infrared Spectroscopy”. Part 1. Instrumentation. Topics in Chemical Instrumentation. Ed. Frank A. Settle, Jr. Journal of Chemical Education, 63:1, A5-A10

[59] K. Inouye, R. Endo, Y. Otsuka, K. Miyashiro, K. Kaneko, T. Ishikawa, J. Phys Chem. 86 (1982) 1465

[60]http://www.the-scientist.com/?articles.view/articleNo/18797/title/Across-the-Spectrum--Instrumentation-for-UV-Vis-Spectrophotometry

[61] http://www.buzzle.com/articles/lcr-meter-working-principle-and-uses.html, in

[62] http://www.radio-electronics.com/info/t_and_m/lcr-meter/basics-tutorial.php, in

[63] S. A. Saafan, Physica B. 403(2008), pp. 2049

[64] K. Mukherjee, S.B. Majumder, Analyses of response and recovery kinetics of zinc ferrite as hydrogen gas sensor, J. Appl. Phys. 106 (2009) 064912–65010

[65] K. Murakami, S. Yasunaga, S. Sunahara, K. Ihokura, Proceedings of the First International Meeting of Chemical Sensors, Fukuoka, Japan, 19–22 September, 1983, pp. 18–23

[66] Y.S. Shen, T.S. Zhang, Sens. Actuat. B 12 (1993) 5

[67] X.F. Chu, X.Q. Liu, G.Y. Meng, Mater. Sci. Eng. B 64 (1999) 60

[68] P.B. Pandya, H.H. Joshi, R.G. Kulkarni, J. Mater. Sci. Lett. 10 (1991) 471

[69] Konicki W, Sibera D, Mijowska E, Lendzion-Bieluń Z, Narkiewicz U. Equilibrium and kinetic studies on acid dye Acid Red 88 adsorption by magnetic ZnFe 2 O 4 spinel ferrite nanoparticles. Journal of colloid and interface science. 2013 May 15;398:152-60

[70] K. Murakami, S. Yasunaga, S. Sunahara, K. Ihokura, Proceedings of the First International Meeting of Chemical Sensors, Fukuoka, Japan, 19–22 September, 1983, pp. 18–23

[71] S.W. Tao, Q.Y. Wu, Z.L. Zhan, G.Y. Meng, Sol. State Ion. 124 (1999) 53

[72] Rita John, S. Sasi Florence, Chalcogenide Lett.6, 535, 2009

[73] Jo-Yong Park, Yun-Jo Lee, Ki-Won Jun, Jin-Ook Baeg, Dae Jae Yim, J.of Ind. and Eng Chem. 12, 882, 2006

[74] J.F. Banfield, Aggregation-Based Crystal Growth and Microstructure Development in Natural Iron Oxyhydroxide Biomineralization Products, Science, 289 (2000) 751-754

[75] Johnstone, J. H. L., and John Warren Williams. "The variation of dielectric constant with frequency." Physical Review 34.11 (1929): 1483

[76] Koops, C. G. "On the dispersion of resistivity and dielectric constant of some semiconductors at audio frequencies." Physical Review 83.1 (1951): 121

[77] Gul, I. H., et al. "Structural, magnetic and electrical properties of $Co_{1-x}Zn_xFe_2O_4$ synthesized by co-precipitation method." Journal of Magnetism and Magnetic Materials 311.2 (2007): 494-499

[78] Funke, K., Radha D. Banhatti, and C. Cramer. "Correlated ionic hopping processes in crystalline and glassy electrolytes resulting in MIGRATION-type and nearly-constant-loss-type conductivities." Physical Chemistry Chemical Physics 7.1 (2005): 157-165

[79] Moulson, Anthony and John M. Herbert. Electroceramics: materials, properties, applications. John Wiley & Sons, 2003

[80] Ravinder, D., and K. Vijaya Kumar. "Dielectric behaviour of erbium substituted Mn-Zn ferrites." Bulletin of Materials Science 24.5 (2001): 505-509

[81] Konaka, Tsuneo, et al. "Relative permittivity and dielectric loss tangent of substrate materials for high-T c superconducting film." Journal of Superconductivity 4.4 (1991): 283-288

[82] Müller, Jürgen G., et al. "The role of exciton hopping and direct energy transfer in the efficient quenching of conjugated polyelectrolytes." Journal of the American Chemical Society 128.12 (2006): 4007-4016